

Article

Prediction of the Turbidity Distribution Characteristics in a Semi-Enclosed Estuary Based on the Machine Learning

Nam-Hoon Kim ^{1,*}, Dong Hyeon Kim ² and Sung-Hwan Park ¹ 

¹ Coastal Disaster & Safety Research Department, Sea Power Enhancement Research Division, Korea Institute of Ocean Science & Technology, Busan 49111, Republic of Korea; spark@kiost.ac.kr

² Institute of Engineering Research, Seoul National University, Seoul 08826, Republic of Korea; email@snu.ac.kr

* Correspondence: nhkim0426@kiost.ac.kr; Tel.: +82-51-664-3708

Abstract: This study addresses the critical challenge of predicting sediment behavior in a semi-enclosed estuary, where the interplay between artificial freshwater discharge and seawater significantly impacts turbidity. Such environments are characterized by complex hydrodynamic interactions that lead to cycles of sediment settling and resuspension, influenced by tidal forces. To tackle this problem, we employed machine learning, leveraging its capability to analyze and predict complex non-linear phenomena. Our approach involved extensive transect observations conducted over two years, encompassing 11 ebb tide and 9 flood tide cycles. These observations were crucial for training the machine learning model, ensuring it captured the nuanced dynamics of sediment behavior under varying hydrodynamic conditions. The necessity of this research lies in its potential to enhance our understanding of sediment dynamics in estuaries, a vital aspect for environmental management and engineering projects. The findings demonstrate a promising alignment between the machine learning model's predictions and the theoretically assumed sediment behavior, highlighting the model's effectiveness in deciphering and predicting turbidity patterns in these challenging environments.

Keywords: semi-enclosed estuary; moving vessel profiling; multi-layer perceptron; turbidity; sediment



Citation: Kim, N.-H.; Kim, D.H.; Park, S.-H. Prediction of the Turbidity Distribution Characteristics in a Semi-Enclosed Estuary Based on the Machine Learning. *Water* **2024**, *16*, 61. <https://doi.org/10.3390/w16010061>

Academic Editors: Jun Song Kim, Dong-Kyun Kim and Donghae Baek

Received: 30 November 2023

Revised: 18 December 2023

Accepted: 21 December 2023

Published: 23 December 2023



Copyright: © 2023 by the authors. Licensee MDPI, Basel, Switzerland. This article is an open access article distributed under the terms and conditions of the Creative Commons Attribution (CC BY) license (<https://creativecommons.org/licenses/by/4.0/>).

1. Introduction

An estuary refers to a dynamic environment where freshwater from rivers mixes with saltwater from the ocean, creating gradients in salinity, nutrient levels, and sediment loads. The extent of hydrodynamics is determined by factors, such as the size and shape of estuary, sediment characteristics, bathymetry, river discharge, as well as wind, waves, and tides [1,2]. In the realm of estuarine classification, estuaries are categorized into three distinct types: open estuary, semi-enclosed estuary, and closed estuary. This is based on their configuration regarding the connection between riverine and marine environments. Among them, a semi-enclosed estuary refers to an estuarine system that has been partially enclosed from direct exposure between the river and sea through the construction of sea-dike with sluice gates. The sea-dike with sluice gates, often constructed for flood control, water storage, and energy generation, significantly alters the natural dynamics of estuaries. The sea-dike inhibits the tidal momentum of the offshore sea from advecting to the river and near coastal waters and, therefore, significantly affects the physical characteristics of the estuaries, such as stratification, mixing, and circulation [1,3,4]. Generally, estuaries are influenced by freshwater, so they have a stratified structure with freshwater in the upper layer and sea water in the lower layer [5]. However, in the case of a semi-enclosed estuary, the characteristics differ slightly from a normal state, as the river and sea are separated by a sea-dike. Particularly during the flood season, the artificial gate operation leads to the discharge of freshwater, which flows into the sea, significantly altering the estuarine circulation from its normal state. During the dry season, the infrequent release of freshwater makes estuarine circulation primarily governed by tidal modulations. The vertical structure

of the water column in estuaries frequently exhibits recursive patterns due to the combined effects of tidal modulations and straining by the advection of river flow. In other words, mixing and stratification occur repetitively, governed by the amplitude of tides with various cycles and phases, as well as by the volume of discharged freshwater. During the flood tide, strong barotropic currents result in the vertical mixing of the water body. During the ebb tide, as freshwater advects over the seawater, a horizontal density gradient tilts towards the sea. This, in turn, leads to the generation of baroclinic currents due to vertical straining, which results in the formation of strong stratification. Generally, baroclinic currents, stemming from vertical differences in water properties such as temperature and salinity, lead to the formation of vertical density structures and potentially complex turbulent flows in estuaries. In contrast, barotropic currents, which are not affected by density differences, are primarily driven by external forces such as wind and tide and can also result in strong turbulence within these environments. This periodic stratification process can be defined as strain-induced periodic stratification (SIPS) [5].

Estuaries often have high turbidity due to the mixing of riverine sediments. Particularly, in macrotidal estuaries where tidal forces are dominant, the presence of the sea-dike not only poses a critical interference in the natural sedimentary processes but also affects sediment transport and deposition patterns due to the discharge of freshwater from artificial gate operation [6]. When gates are opened, there may be sudden pulses of sediment and freshwater that create plumes and turbidity currents, differing from the usual gradual mixing processes. Over time, the discharged sediments undergo repeated cycles of settling and resuspension, driven by tidal modulations, resulting in very complex bathymetry changes. The tidal-driven barotropic currents, potentially due to flood tides, might resuspend sediments, while the density-driven baroclinic currents, particularly driven by ebb tides, can influence where these sediments settle or are transported vertically [7]. The behavior characteristics of sediments according to the vertical structure of these water columns have already been theoretically proven through numerical models and observations [8–10]. Understanding and predicting the behavior of sediments in estuaries are crucial due to their impact on several key environmental factors. Firstly, they affect light occlusion, which, in turn, influences primary production. Primary production is the creation of organic compounds from carbon dioxide through photosynthesis, primarily by plants and algae. When suspended sediments block or reduce light penetration in water, they can significantly affect the growth and health of these photosynthetic organisms. Secondly, suspended sediments serve as pathways for adsorbed contaminants. These particulates can bind with various contaminants, including heavy metals and organic pollutants, transporting them through the estuarine environment. This transportation can impact water quality and the health of aquatic ecosystems, making it a critical area of study. Lastly, the concentrations of these particulates play a role in the rates of accretion and erosion, impacting the bathymetric evolution of estuaries. Bathymetry is essential in understanding how estuaries change over time. Changes in the rates of accretion and erosion can alter the physical structure of estuaries, affecting their ecological dynamics and the organisms that inhabit them. Therefore, understanding and predicting the behavior of suspended sediments in estuaries are vital for ecological conservation, managing water quality, and maintaining the health of these unique environments.

In order to understand and predict the sediment behavior in estuaries, we adopt the on-site survey and machine learning task. The simulation of the sediment behavior in estuaries has primarily been conducted using process-based models that are grounded in mathematics and physics. These models are based on theoretical principles and simulated physically and mathematically, making them very useful tools for understanding basic processes. However, they require observational data for the validation of simulation results, and the results may not be reliable without sufficient observational data. On the other hand, data-driven models, such as machine learning, can directly utilize actual observational data. If these models include detailed interpretations, they can predict the fundamental processes of phenomena with high reliability. Therefore, in this study, we aim to validate

the theoretical background of these phenomena through observation and establish a data-driven machine learning model that directly utilizes these theories to validate the theoretical background. The objectives of this study are: (1) to conduct transect observations in a semi-enclosed estuary to acquire data, (2) to analyze these data to theoretically verify the characteristics of the water column and the relationship with sediments according to tidal modulations, and (3) to use the collected data to perform neural network-based machine learning, thereby predicting the settling and resuspension characteristics of sediments in response to tidal modulations.

2. Materials and Methods

2.1. Study Area

The Geum River Estuary (GRE) is located at the confluence of the Geum River and the Yellow Sea in South Korea (Figure 1). The sea-dike is at the mouth of the Geum River, which is the third-largest river in South Korea. The sea-dike itself is a notable structure, spanning a length of 1841 m and consisting of 20 sluice gates, each 30 m in width and 10.3 m in height. The GRE has a width of approximately 2 km and a navigation channel of about 23 km from the sea-dike to the north breakwater. The water depth is mostly shallower than 20 m, and extensive tidal flats exist. Also, the GRE is subject to complex tidal dynamics due to its semidiurnal macrotidal environment, where the tidal range is about 2.8–6.0 m [11]. The freshwater is discharged irregularly and artificially through the sluice gates of the sea-dike, depending on the water level upstream of the reservoir, rainfall, tidal phase, and the capacity of water storage of the sea-dike [12]. The operators analyze multiple pieces of information comprehensively to make flexible decision making about discharging water. Generally, during discharge, all 20 sluice gates are opened, with 1–2 m of opening height. The sea-dike was constructed in 1994, making a significant shift in the hydrodynamics and sediment transport characteristics of the estuary. Before the construction of the sea-dike, tidal flows were predominantly governed by mixing and stratification processes. However, post-construction, the artificial discharge of freshwater is irregular and typically occurs only during ebb tides, contingent on the reservoir water levels. Although it exhibits characteristics distinct from typical estuaries, being a semi-enclosed estuary, the repeated mixing and stratification due to tidal modulations after artificial freshwater discharge imply that the GRE can be categorized as a SIPS condition [7]. Furthermore, the grain size in the GRE changed from sandy to muddy following the construction of the sea-dike [13]. The particle size refinement could lead to most sediments being trapped and deposited within the estuary [11].

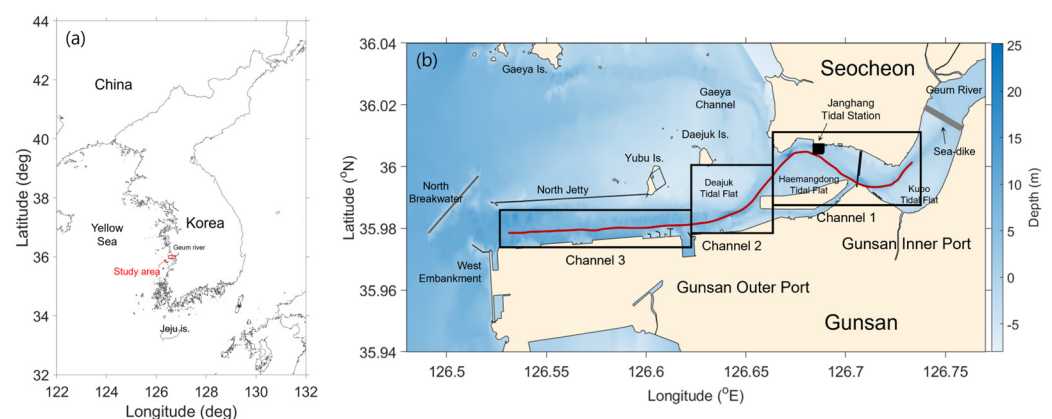


Figure 1. (a) Location of the study area and (b) detail description of the GRE.

Historically, the GRE has undergone significant changes, especially after the construction of the sea-dike. This structure has altered the natural flow and sediment deposition patterns, affecting the estuarine dynamics. These alterations have implications for the sediment behavior, including changes in turbidity patterns and sediment transport mecha-

nisms. The estuary experiences a complex interplay of freshwater from the Geum River and saltwater from the Yellow Sea, leading to unique hydrodynamic conditions. This interaction results in significant tidal influences, with pronounced variations in sediment settling and resuspension behaviors during ebb and flood tides. The semi-enclosed nature of the estuary, combined with the influence of the sea-dike and the tidal modulations, presents an ideal setting for investigating the sediment dynamics influenced by artificial structures and natural tidal forces. Understanding these dynamics is crucial for environmental management, particularly in regions undergoing rapid industrialization and urbanization, as is the case with many estuarine environments globally. The GRE is not just a critical hydrological feature but also an important ecological habitat. It supports a diverse range of aquatic and terrestrial species, making it a key area for biodiversity. The estuary's ecological significance is further emphasized by its role in the life cycles of various fish species and as a vital stopover for migratory birds.

2.2. Data Acquisition

The on-site surveys were conducted along the navigation channel for each ebb and flood tide after freshwater discharge. The data were acquired through transect observations using the Moving Vessel Profiler (MVP) method. The MVP is an in situ survey method employing a Lagrangian approach [14,15]. It involves mounting several measurement instruments to the vessel to acquire ocean variables. So, it allows for the rapid collection of environmental data from a moving vessel, significantly improving the efficiency and coverage of data collection.

Acoustic Doppler Current Profiler (ADCP) and Yoing Ocean Data Acquisition profiler (YODA profiler) were mounted on the vessel to measure hydrodynamics and water properties (Figure 2). The M9 ADCP (Sontek) can collect three-dimensional velocity (Eastward, Northward, Upward velocity, VelENU) profiles over an available depth range. It features nine beams: one vertical beam operating at a 500 kHz frequency and two sets of four slanted beams operating at 1 and 3 MHz, respectively. Additionally, a DGPS system is operated concurrently, allowing for the simultaneous recording of real-time positional information. Integrating DGPS with M9 ADCP ensures accurate spatial referencing of the collected oceanographic data. Such an integrated system was mounted on the side of the vessel using a custom-designed mounting frame. This setup facilitated the efficient operation of the system, allowing for the seamless collection of oceanographic data. The YODA profiler is a free-fall towed profiling system that can acquire high-resolution water column data [16]. A brush is mounted at the top of the profiler, which promotes a stable, uniform sinking velocity in free-fall mode. The main body consists of a RINKO-Profiler (JFE Advantech Co., Ltd.), which carries a thermistor (water temperature), electrode (conductivity, Cond), semiconductor pressure sensor (depth), fluorimeter (Chlorophyll, Chl-a), backscattering (turbidity, Turb), and phosphorescence (dissolved oxygen, DO) sensors mounted at the bottom of the profiler. Salinity is calculated based on the Practical Salinity Scale of 1978 (PSS-78) using conductivity, temperature, and pressure. Then, density (σ_t) is calculated based on PSS-78 using temperature, salinity, and pressure. A winch is mounted on the stern of the vessel to support the profiling of the YODA system. This setup enables the precise lowering and raising of the YODA profiler into the water, facilitating accurate and efficient data collection.

The horizontal and vertical resolutions of the M9 ADCP and YODA systems are influenced by both the boat speed and the water depth (Table 1). In order to guarantee stable data acquisition, the boat speed was consistently maintained between 2 and 3 knots (1.0–1.5 m/s). The M9 ADCP, recording data at a frequency of 1 Hz, achieves a horizontal resolution of approximately 1–1.5 m. It uses three acoustic frequencies and employs the SmartPulseHD algorithm to select the most suitable frequency based on the boat's speed and water depth. Consequently, the vertical resolution of the M9 ADCP ranges from about 0.02 m to 4 m. The YODA profiler operates with a sampling frequency of 10 Hz and observes the vertical structure of the water properties with a resolution of approximately 0.02–0.03 m.

This is achieved by adjusting the sinking speed to 0.2–0.3 m/s. This configuration allows the profiler to capture fine-scale variations in the water column, providing detailed insights into its vertical structure.

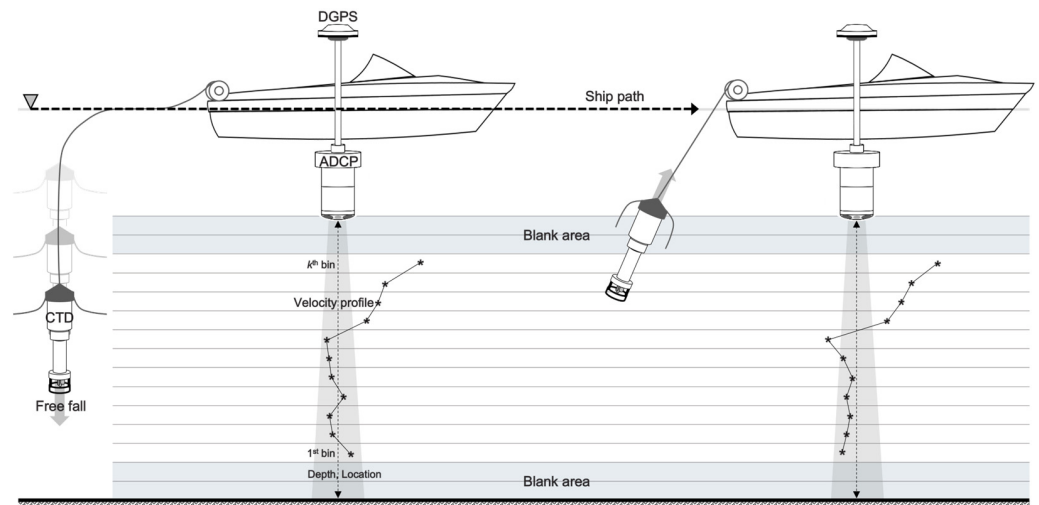


Figure 2. Schematics of the MVP method mounting the ADCP and YODA on the vessel.

Table 1. Descriptions of the ADCP and YODA profiler.

Instruments	Variables	Resolution	Accuracy
ADCP	Time Water depth Longitude Latitude Velocity ENU	Horizontal: 1 m to 1.5 m Vertical: 0.02 m to 4 m	Water depth: 0.02 m DGPS: <1.0 m Velocity: ± 0.2 cm/s
YODA	Time Water depth Water temperature Density (Sigma-t) Conductivity (Cond) Chlorophyll-a (Chl-a) Dissolved Oxygen (DO) Turbidity (Turb) (Salinity)	Horizontal: # of profiles Vertical: 0.02–0.03 m	Water temperature: ± 0.01 °C DO: $\pm 2\%$ FS (FS: Air saturation 0 to 200%) Depth: $\pm 0.3\%$ FS (FS: 0 to 600 m) Cond: ± 0.01 mS/cm ⁻¹ Turb: ± 0.3 FTU Chl-a: $\pm 1\%$ FS (FS: 0 to 400 ppb)

2.3. Multi-Layer Perceptron Neural Network (MLP-NN)

The Multi-Layer Perceptron Neural Network (MLP-NN) model mimics the human brain’s synaptic neuron system and has many applications in water research. MLP-NN trains an approximation of a nonlinear regression function by mapping n -feature vectors to corresponding target vectors through several hidden layers. It is a multi-variable regression model based on neural networks designed to predict corresponding target vectors. The input layer comprises n -feature vectors, while the output is formed by target vectors. The hidden layer acts as an intermediary, connecting the input and output. Composed of multiple nodes, each equipped with weights and biases, the hidden layer in a multilayer structure facilitates the transmission of information between nodes of adjacent layers. The MLP-NN model constructed in this study is a feedforward neural network, and its architecture and descriptions are presented in Figure 3 and Table 2.

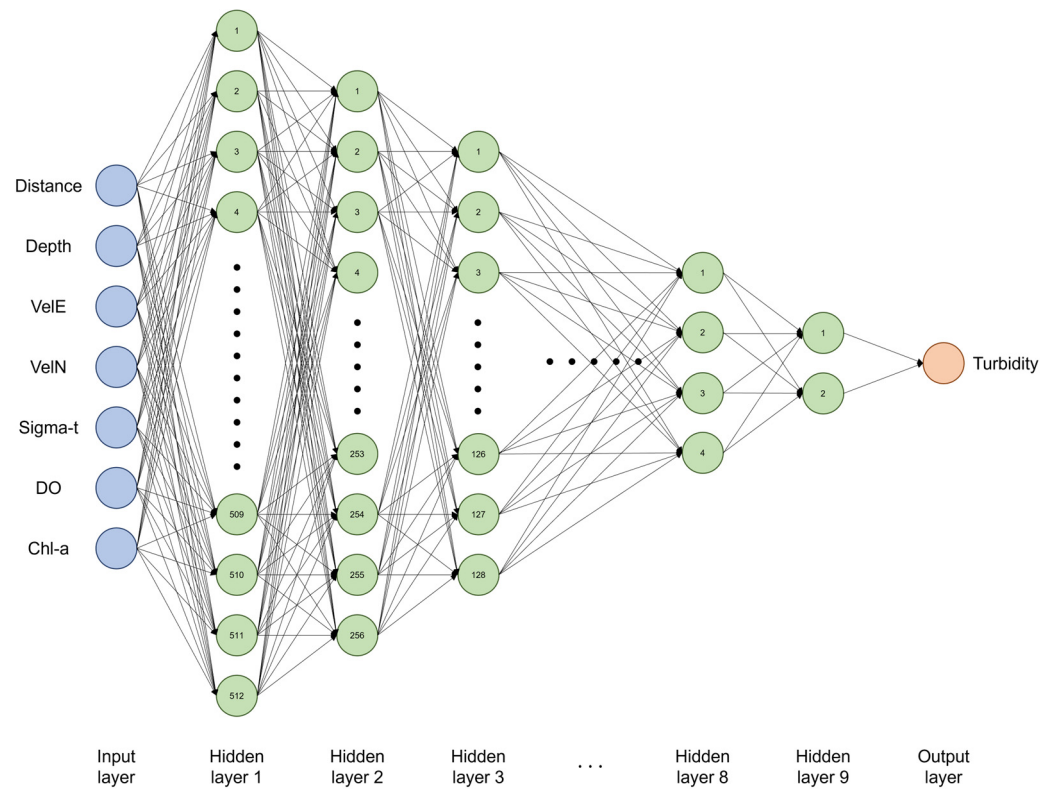


Figure 3. The architecture of the MLP-NN model.

Table 2. Descriptions of the MLP-NN model.

Contents	Setting
Input variables	7
Data division (Training/Validation/Test)	0.7/0.15/0.15 (randomly)
# of hidden layers	8 [512, 256, 128, 64, 32, 16, 8, 4, 2, 1]
[# of nodes for each hidden layer]	
Output variables	1
Activation function	(each layer) tansig/(output layer) purelin
Objective function	Mean Squared Error (MSE)
Training function	Scaled conjugate gradient algorithm
Learning rate	10^{-6}
Max epochs	1000

The MLP-NN model utilizes seven hydrodynamic and water property parameters from transect observations based on the MVP method as input. The model is trained to predict turbidity as the output. The data are distributed across training, validation, and test, comprising 70%, 15%, and 15% of the dataset, respectively, with random sampling employed during the training process. Each variable corresponding to the input values was subjected to min–max normalization. The hidden layers are designed with 10 layers, each reducing the number of nodes by half, starting from 512 and descending to 1. The transfer function of each hidden layer is set as a tansig function, a hyperbolic tangent sigmoid transfer function. This function outputs values in the range $[-1, 1]$. It is commonly used in neural networks due to its smooth, nonlinear characteristics, which allow the network to capture and model complex relationships in the data. For the output layer, the activation function is a purelin function, which is a linear transfer function. This is appropriate for regression tasks as it allows the network to output a wide range of real-valued numbers, matching the nature of most regression targets. For performance evaluation, the objective function was constituted using Mean Squared Error (MSE), and

optimization of the objective function utilized the scaled conjugate gradient algorithm to enhance GPU computing efficiency for Jacobian matrices. The dataset used for the training is not too big, so we adopt a form of batch training in which the network processes all training examples at once rather than dividing data into mini-batches.

3. Results

3.1. Transect Observations Based on the MVP Method

Transect observations based on the MVP were conducted along the navigation channel, which spans approximately 23 km from the sea-dike to the north breakwater. Observations were conducted during ebb and flood tides, based on the time elapsed after the artificial discharge of freshwater. During the observation period, external environmental factors such as weather and vessel traffic influenced the success of data acquisition across the entire navigation channel. Consequently, there were days when successful data acquisition was achieved throughout the navigation channel, while on other days, it was not. Therefore, it was impossible to obtain spatially consistent data for all observations. Tables 3 and 4 summarize the observation details and data acquisition status from March 2015 to January 2017, according to different tidal conditions. Each observation was conducted between a minimum of 11 h and a maximum of 153 h after freshwater discharge, and detailed information regarding the freshwater discharges prior to each observation is presented in Table A1. Due to spatial inconsistencies, the area extending from the north breakwater to the sea-dike was divided into three regions (Figure 1). The data acquisition status was separately identified for each of these regions. During the ebb tide, observations began near the north breakwater and progressed towards the sea-dike, while during flood tides, the process was reversed. This method is adopted because, during the ebb tide, the water near the sea-dike recedes towards the open sea, exposing the intertidal zone and tidal flats extensively and reducing the observable water depth significantly, thereby making it impractical to conduct observations from the sea-dike towards the open sea. Conversely, during the flood tide, the water depth near the sea-dike increases sufficiently, facilitating observations from the sea-dike towards the open sea.

Table 3. Description of the transect observations during ebb tide.

No.	Date	Time after Freshwater Discharge (h)	C1	C2	C3	# of Profiles
1	2015.03.14.	26	O	X	X	49
2	2015.04.11.	24	O	O	O	135
3	2015.08.24.	72	O	O	O	181
4	2016.01.14.	129	O	X	X	64
5	2016.01.15.	153	X	O	O	82
6	2016.09.02.	11	O	O	O	94
7	2016.09.02.	19	X	X	O	16
8	2016.11.10.	75	O	O	X	69
9	2016.11.11.	24	O	O	O	89
10	2017.01.07.	21	O	O	O	144
11	2017.01.08.	46	O	O	O	153
Sum						1076

When ADCP and YODA are simultaneously mounted on a vessel for observation, ADCP acquires continuous water column data, while YODA collects profile data. Moreover, since YODA lacks position information, synchronization with ADCP data is necessary to determine the profile positions. GPS data were logged concurrently with the ADCP measurements and were used to synchronize the data from both the ADCP and the YODA profiler based on the recorded times. Therefore, the positional information of YODA profiles is extracted from the ADCP based on synchronizing the recorded times in both ADCP and YODA data. Additionally, as the MLP-NN to be presented later involves preprocessing the input values based on YODA profiles, ADCP profile data were also extracted from the same

positions as the YODA profiles to maintain positional consistency. The extracted ADCP profiles and YODA profiles possess different vertical resolutions. Notably, the M9 ADCP, due to its SmartPulseHD algorithm, has a variable vertical bin size and exhibits blank spaces near the surface and bottom (Figure 2). In contrast, YODA can observe from near-surface depths down to the bottom, providing relatively high-resolution and comprehensive depth information. Since the MLP-NN requires input data of uniform length for training, we standardized the resolution of all profiles to 100 points, primarily based on the depths where ADCP data begin and end, to align the dimensions of the two datasets.

Table 4. Description of the transect observations during flood tide.

No.	Date	Time after Freshwater Discharge (h)	C1	C2	C3	# of Profiles
1	2016.01.14.	133	O	X	X	67
2	2016.03.22.	133	O	O	O	137
3	2016.09.01.	70	X	O	O	105
4	2016.09.02.	15	O	O	O	101
5	2016.09.02.	18	X	X	O	25
6	2016.11.10.	71	O	O	X	80
7	2017.01.10.	92	O	O	O	164
8	2017.01.11.	15	O	O	O	183
9	2017.01.12.	40	O	O	O	127
Sum						989

The observation results presented henceforth represent only representative cases, with additional data provided in Appendix A (Figures A1–A15). These cases are derived from consecutive transect observations conducted over five days: 7, 8, 10–12 January 2017 (Figure 4). Among these, the observations on 7 and 8 January were conducted during the ebb tide, approximately 21 and 46 h, respectively, after freshwater discharge. The observations on 10–12 January were carried out during the flood tide, about 92, 15, and 40 h post-discharge, respectively. The variables displayed in the figure include x- and y-directional velocities (VelE and Vel N), sigma-t, Chl-a, DO, and Turb, which are directly utilized in the machine learning described later. Additionally, the gradient Richardson number (Ri_g) along the observation transect was included in the figures. The Ri_g is a dimensionless number defined as the ratio of buoyancy to shear ($Ri_g = N^2/S^2$). It is significant in determining the stability of the flow. A high Ri_g indicates stable stratification where buoyancy suppresses turbulence, while a low Richardson number suggests that shear forces dominate, leading to turbulent flow. Generally, a Ri_g below a critical value ($Ri_c = 0.25$, [17]) indicates that turbulence is likely to occur. In this study, the Ri_g was used to distinguish between stratification and mixing in the water column, dividing it into three ranges: actively mixed condition ($Ri_g < 0.25$), possibly mixed condition ($0.25 < Ri_g < 1$), and stable stratification ($Ri_g > 1$) [18].

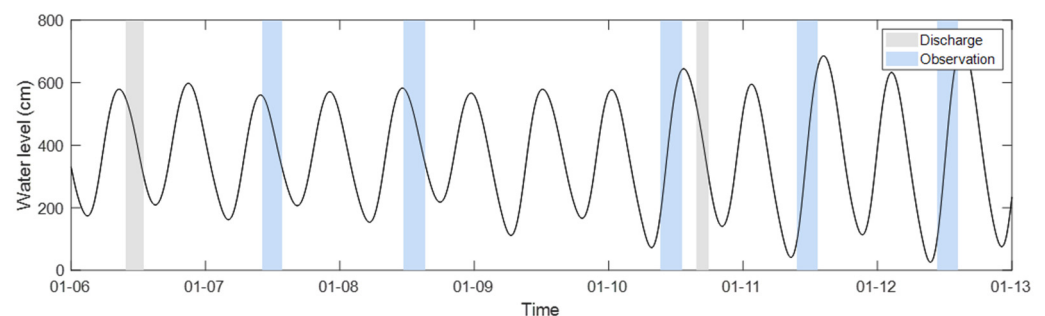


Figure 4. Time series of tidal variation, duration of the freshwater discharge and representative transect observations.

Figures 5 and 6, respectively, show the vertical profiles acquired from transect observations based on the MVP method during ebb tide, 21 h (7 January 2017) and 46 h (8 January 2017) after freshwater discharge. The velocity data obtained from the ADCP during ebb tide predominantly show a westward direction and exhibit a distinct baroclinic flow structure. Relatively higher flow velocities were observed within Channels 2 and 3, approximately 11–18 km away from the sea-dike. Only 21 h after the freshwater discharge, the results obtained from YODA in the area near the sea-dike (Channel 1) clearly reveal information about the freshwater discharge from sigma-t, Chl-a, and DO (Figure 5). Shortly after freshwater discharge, strong stratification is generally observed throughout the water column, yet some mixing characteristics are also apparent in areas close to the sea-dike (Figure 5g). Further, 46 h after the freshwater discharge, it is evident that the water column in Channel 1 is recovering, becoming mixed due to several tidal modulations (Figure 6). Moreover, a more distinct stratification than previously observed formed along parts of Channel 2 and the entirety of Channel 3, while active mixing is evident in Channel 1 and parts of Channel 2 (Figure 6g).

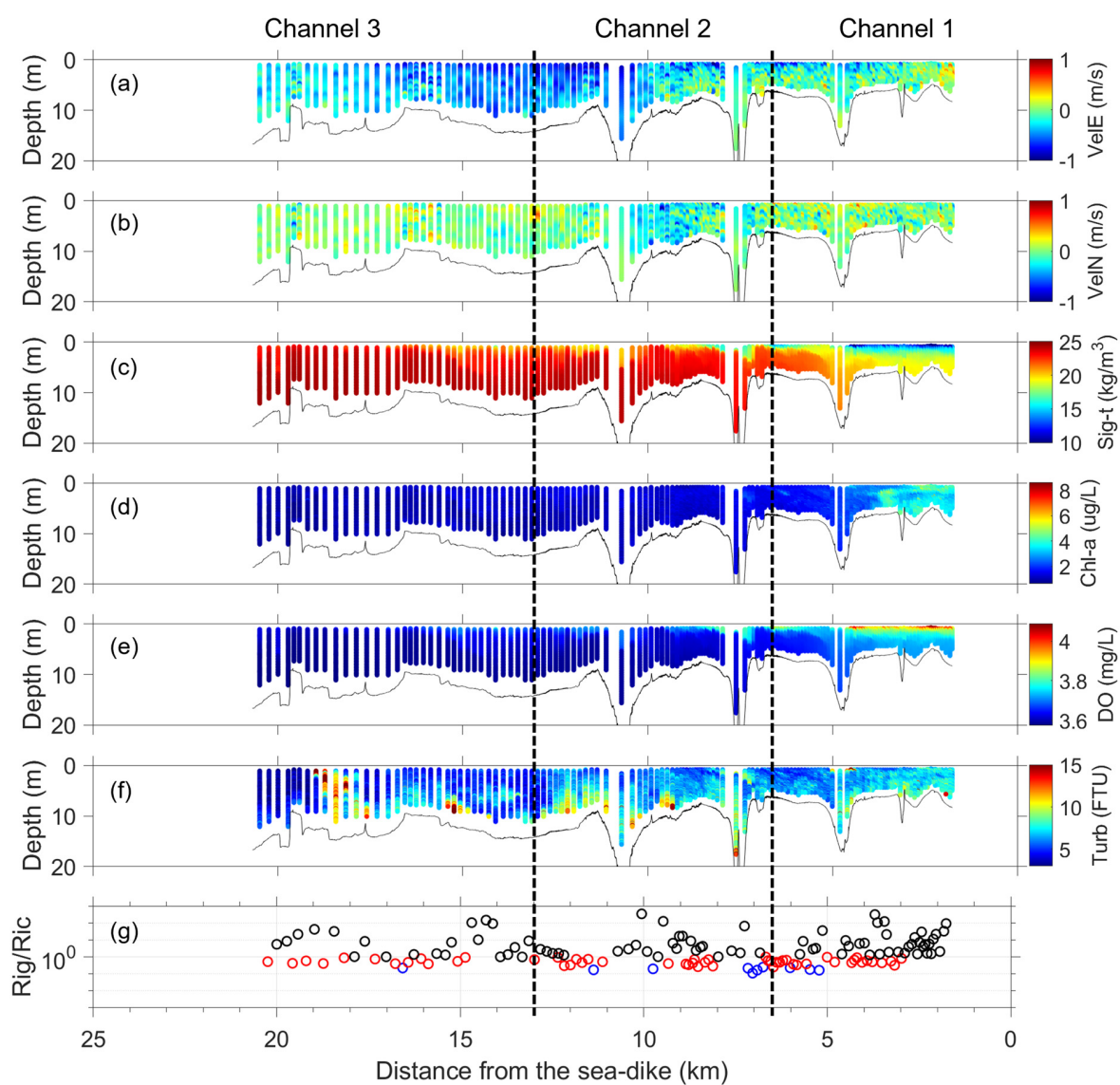


Figure 5. (a–f) Vertical profiles acquired 21 h after freshwater discharge through the transect observation based on MVP method during the ebb tide (7 January 2017). (g) The gradient Richardson number (Ri_g), where blue dots indicate actively mixed conditions, red dots represent possibly mixed conditions, and black dots denote stably stratified conditions.

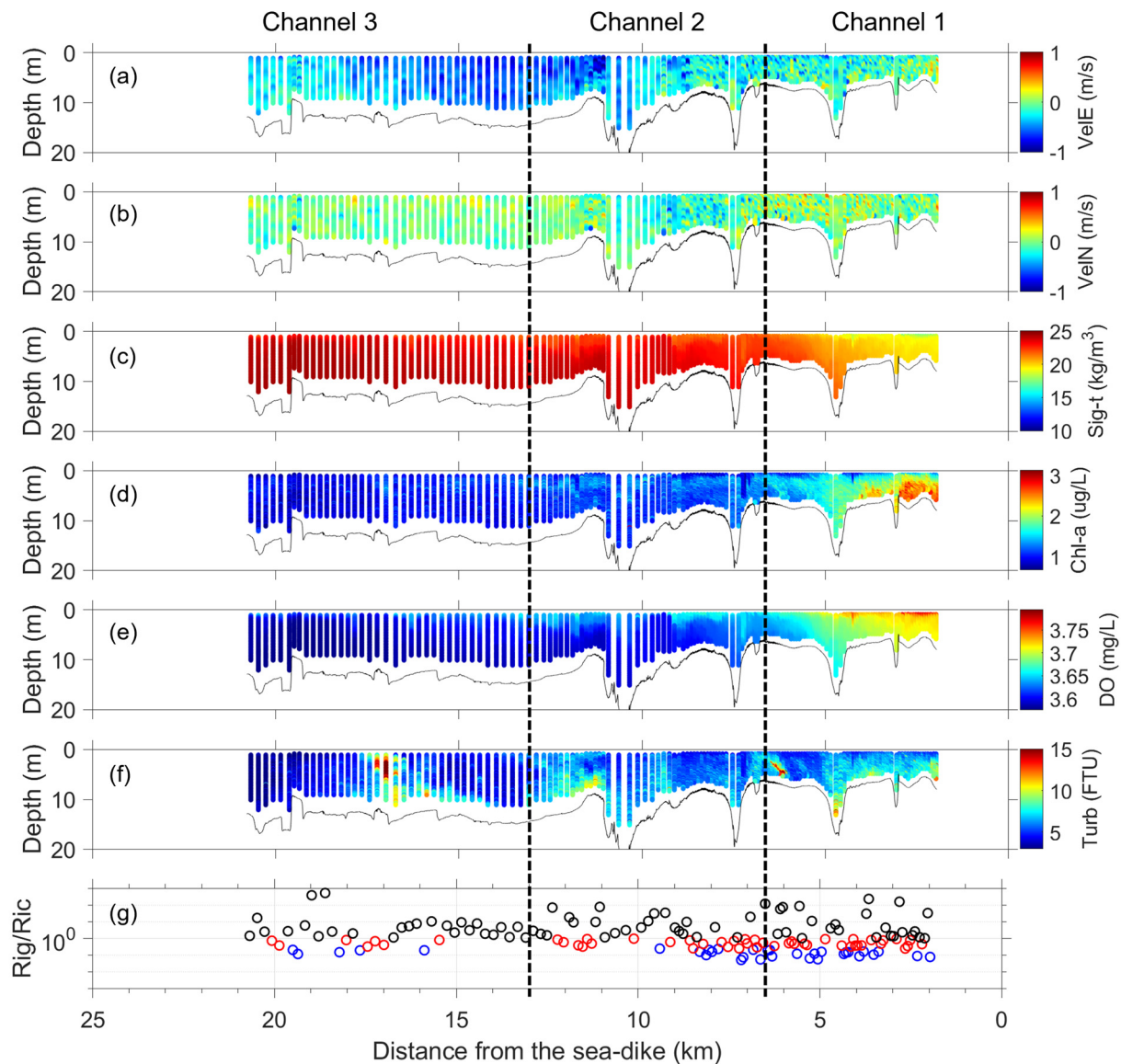


Figure 6. (a–f) Vertical profiles acquired 46 h after freshwater discharge through the transect observation based on MVP method during the ebb tide (8 January 2017). (g) The gradient Richardson number (Ri_g), where blue dots indicate actively mixed conditions, red dots represent possibly mixed conditions, and black dots denote stably stratified conditions.

Figure 7 shows observation data approximately 92 h after the freshwater discharge, and Figures 8 and 9 present observation data from 15 h and 40 h after a subsequent freshwater discharge following the observation of Figure 7. In other words, this means that these are temporally continuous data. The velocity data acquired from the ADCP during flood tide predominantly indicate an eastward direction, showing a barotropic flow structure. Further, 92 h after the freshwater discharge, a weak stratification is visible along all channels, but the majority appears to be mixed (Figure 7). The results of the gradient Richardson number indicate that Channels 1 and 2 are predominantly characterized by mixing, while Channel 3 exhibits a combination of mixing and stratification (Figure 7g). Following the freshwater discharge that occurred 15 h before the start of the next day's observation, subsequent to the previous day's observation, strong freshwater components in sigma-t, Chl-a, and DO were detected in Channel 1, near the sea-dike (Figure 8). This indicates that freshwater is predominantly distributed along the surface shortly after the discharge, leading to strong stratification. However, in Channel 1, there is a general tendency towards active mixing (Figure 8g), and 40 h after the freshwater discharge, corresponding to the next day's

observation, the water column appears to recover in a mixed state (Figure 9). The gradient Richardson number reveals strong stratification in all channels except Channel 1, 15 h after the freshwater discharge (Figure 8g). In contrast, active mixing is observed throughout all channels 40 h post-discharge (Figure 9g).

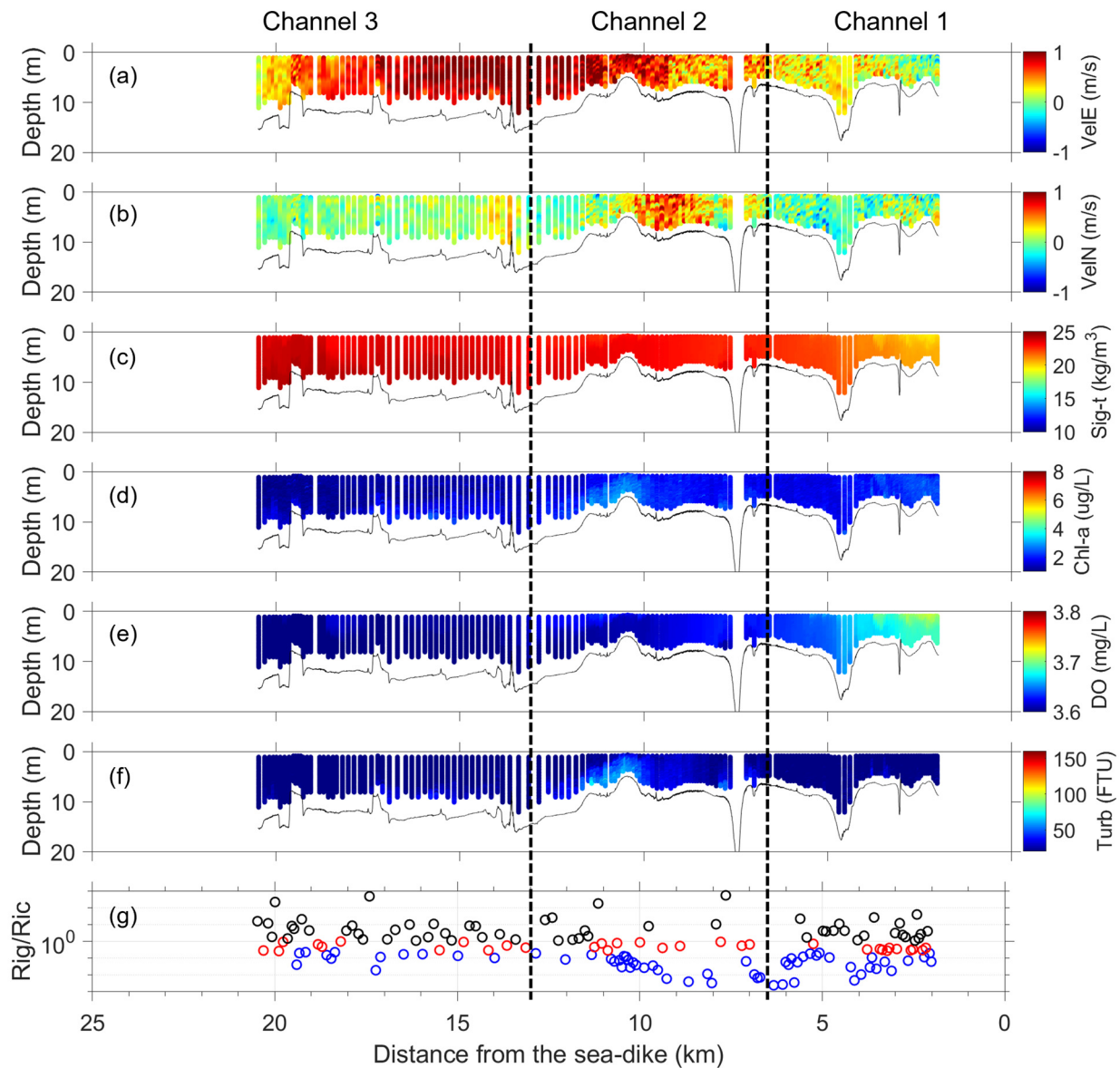


Figure 7. (a–f) Vertical profiles acquired 92 h after freshwater discharge through the transect observation based on MVP method during the flood tide (10 January 2017). (g) The gradient Richardson number (Ri_g), where blue dots indicate actively mixed conditions, red dots represent possibly mixed conditions, and black dots denote stably stratified conditions.

Generally, sediment has a linear relationship with turbidity. We will define sediment dynamics based on the turbidity sensor attached to the YODA profiler. For turbidity, 21 h after freshwater discharge, traces of the discharge seem to persist, as evidenced by the sediment generally appearing to be suspended (Figure 5f). However, 46 h later, the sediment generally appears to settle more than in the previous observation (Figure 6f). Despite the passage of a day, the sediment flew into the outside of the sea-dike together with freshwater or was resuspended by the abrupt energy from the freshwater discharge but still appears to remain suspended due to the formation of a strong mixing layer. In Channels 2 and 3, however, there is a clear indication that the sediment settled more than

the previous day. The high turbidity observed in parts of Channel 3 during the ebb tide is presumed to be influenced by dredging activities occurring at the time of observations. The turbidity characteristics during a flood are completely different from those during ebb tide. Figures 5 and 6, representing ebb tide, show a turbidity range of approximately 3–15 FTU, while the turbidity range during flood tide, as presented in Figures 7–9, is about 30–150 FTU, which is 10-times higher than the ebb tide. This clearly indicates that significant sediment resuspension occurs during flood tide, while sedimentation occurs during ebb tide. Considering the possibility that the observation data might include outliers, these predictive results can be regarded as quite accurate. In summary, while the MLP-NN does not predict the artificially induced suspended characteristics well, irrespective of tidal variations, it is highly effective in predicting the impact of hydrodynamic characteristics inherent in each tidal cycle on sediment behavior.

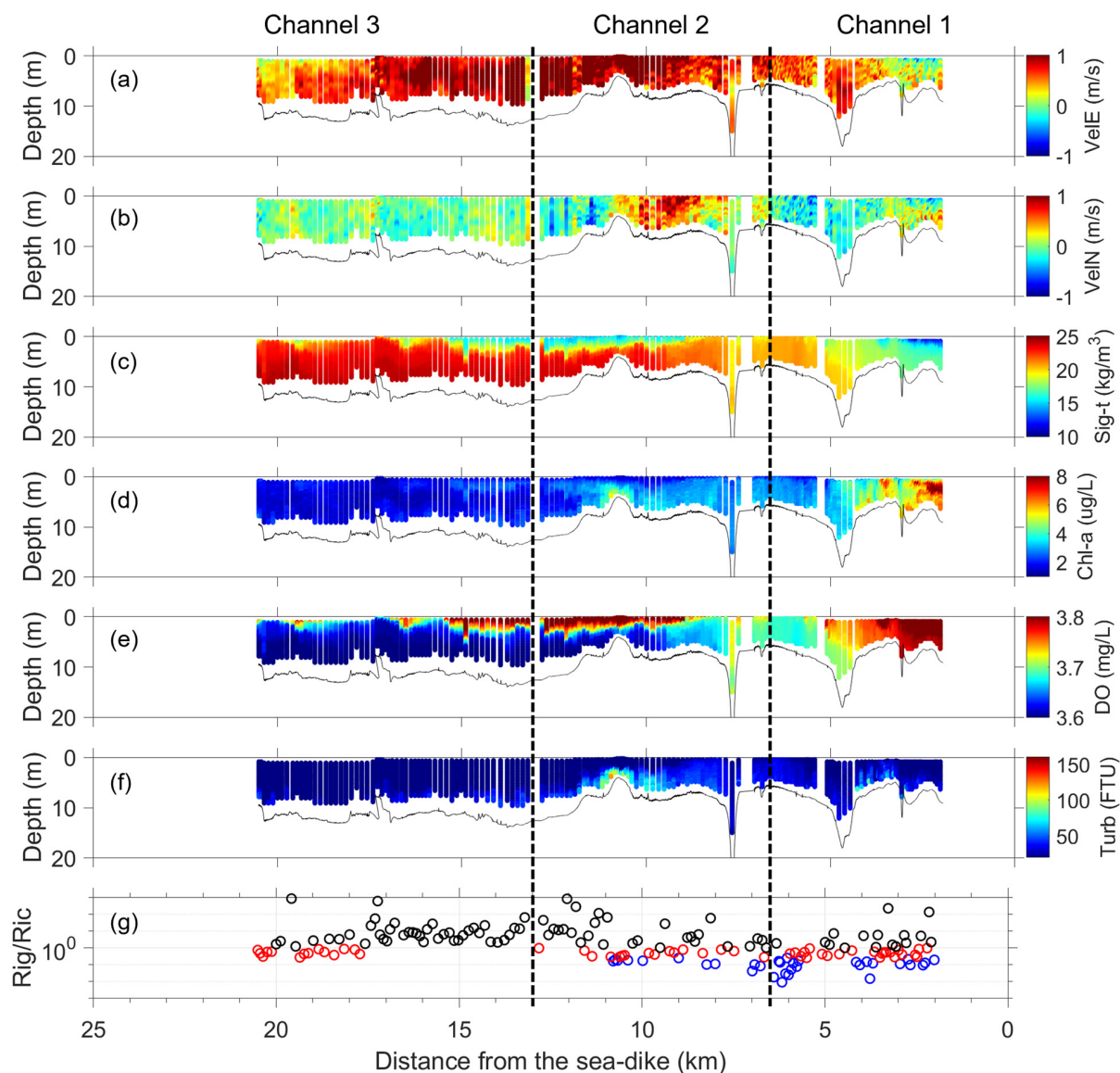


Figure 8. (a–f) Vertical profiles acquired 15 h after freshwater discharge through the transect observation based on MVP method during the flood tide (11 January 2017). (g) The gradient Richardson number (Rig), where blue dots indicate actively mixed conditions, red dots represent possibly mixed conditions, and black dots denote stably stratified conditions.

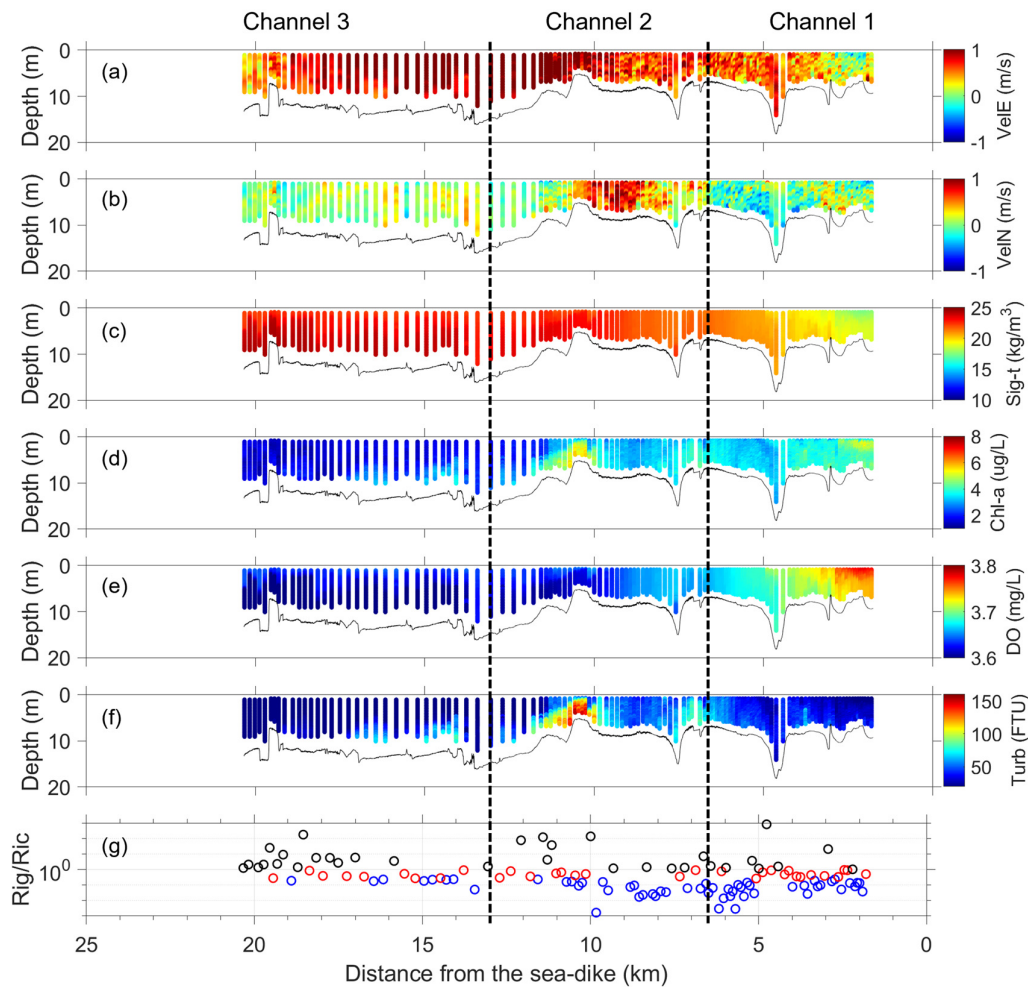


Figure 9. (a–f) Vertical profiles acquired 40 h after freshwater discharge through the transect observation based on MVP method during the flood tide (12 January 2017). (g) The gradient Richardson number (Ri_g), where blue dots indicate actively mixed conditions, red dots represent possibly mixed conditions, and black dots denote stably stratified conditions.

3.2. Estimation of the Turbidity Profiles Using MLP-NN

The representative transect observation data during ebb and flood tides shown in the previous section intriguingly exhibit continuity in the characteristics of the observed variable over time. From this perspective, since 11 and 9 sets of data were accumulated, respectively, during ebb and flood tides from 2015 to 2017, a study was conducted where some of these datasets were used to train a nonlinear regression model based on MLP-NN. The model performance was then validated and tested using a dataset not utilized in the training process.

For training purposes, the data utilized included east–west and north–south current velocities and depth from the ADCP and sigma-t, Chl-a, and DO obtained from YODA, set as input variables, with turbidity as the output variable. Although transect observations were conducted along the 23 km navigation channel, various factors prevented the acquisition of the data across the entire channel. In order to reflect this spatial inconsistency in the training model, distance from the sea-dike calculated retroactively from GPS was also used as an input variable, in addition to ADCP and YODA data. Moreover, to align the dimensions of the ADCP and YODA datasets, the location and vertical resolution of the profiles were standardized.

The training of the MLP-NN model was conducted by splitting the data into separate sets for ebb and flood tide. Then, 923 profile data acquired from 14 March 2015 to 7 January 2017 and 862 profile data acquired from 14 January 2016 to 11 January 2017 were used for

simulation. These datasets were divided into training, validation, and test sets in a 0.7, 0.15, 0.15 ratio, respectively. Ultimately, the performance test of the model for both ebb and flood tide utilized observational data from 8 January 2017 and 12 January 2017, which were not included in the training dataset.

Figures 10 and 11 show the training results of the MLP-NN model. During the ebb tide, the minimum MSE was 4.61 where epochs stopped at 638 (Figure 10a), demonstrating an overall high correlation coefficient (Figure 10b). However, there is a tendency for the output to be underestimated compared to observations in the 20–40 FTU. During the flood tide, the minimum MSE was 15.01 where the epoch stopped at 704 (Figure 11a), demonstrating strong correlation between observations and outputs (Figure 11b). For the test, the data acquired from Figure 6 for the ebb tide and Figure 9 for the flood tide were used as input, and performance evaluation was conducted by comparing with the turbidity data available at that time. Figures 12 and 13 show the test results during ebb and flood tide, respectively. During the ebb tide, it was predicted that sediments would be suspended in Channel 1 very close to the sea-dike, while in the rest of the channels, settling occurred below the mid-layer (Figure 12b). However, when compared with observation data (Figure 12a), predictions in Channel 1 were both underestimated in value and range, and strong turbidity at the 6–7 km was missed. Additionally, turbidity was underestimated around 11–13 km in Channel 2 and around 17–18 km in Channel 3. It was also observed that the turbidity under the mid-layer around 18–21 km in Channel 3 was overestimated. Conversely, during the flood tide, the prediction results were similar to the observation data except for a slight underestimation (Figure 13).

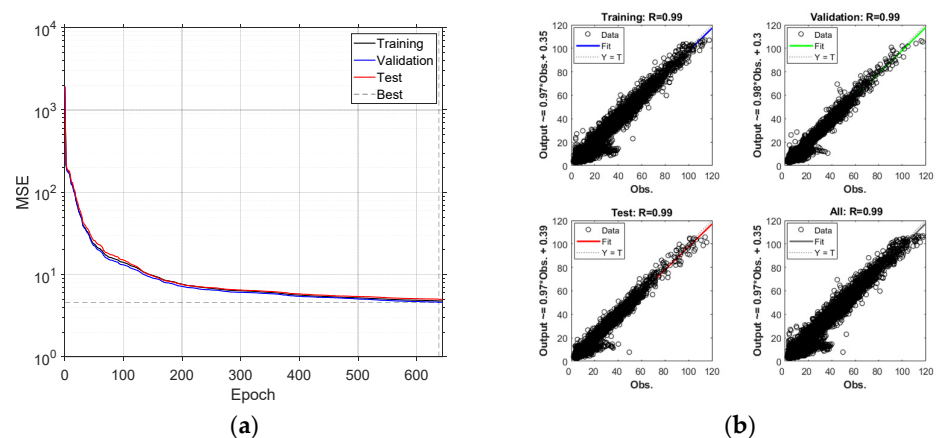


Figure 10. (a) Performance and (b) regression curve of the MLP-NN for predicting the turbidity during ebb tide, showing results for training, validation, and test.

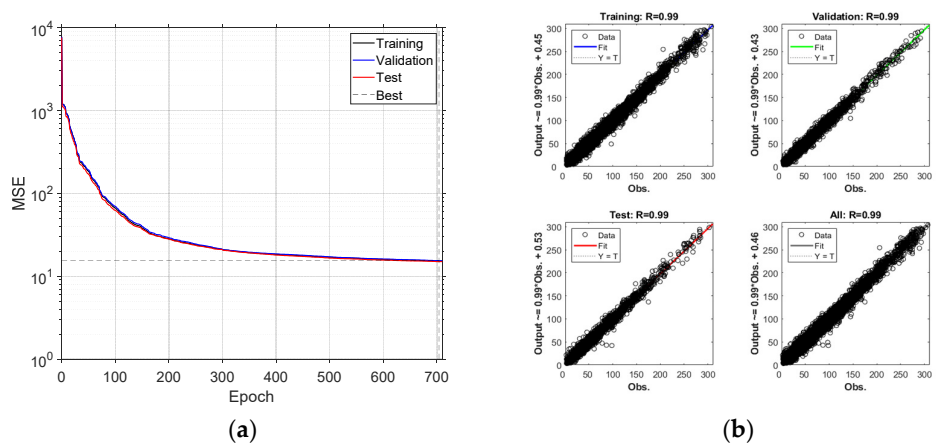


Figure 11. (a) Performance and (b) regression curve of the MLP-NN for predicting the turbidity during flood tide, showing results for training, validation, and test.

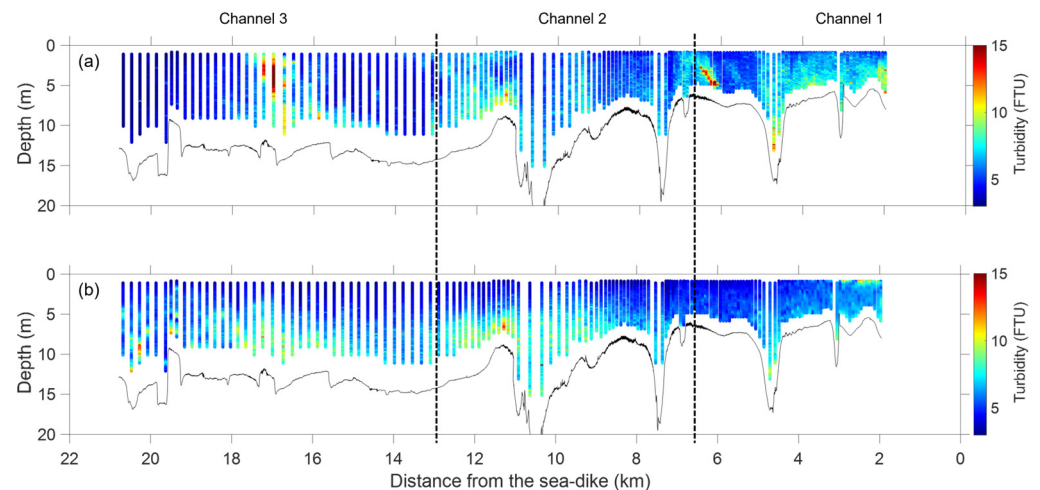


Figure 12. Vertical profiles of (a) observed and (b) predicted turbidity after 46 h of freshwater discharge during ebb tide (8 January 2017).

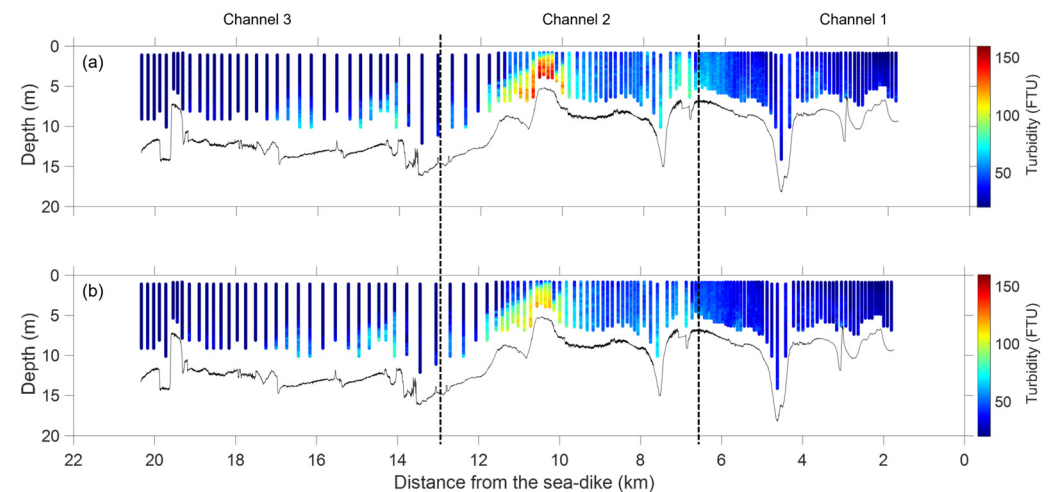


Figure 13. Vertical profiles of (a) observed and (b) predicted turbidity after 46 h of freshwater discharge during flood tide (12 January 2017).

Figure 14 is a scatter plot of the prediction results for ebb and flood tides. During ebb tides, the correlation was approximately 0.31 between the predictions and the actual observations. It was noted that high turbidity levels of 10–15 FTU were underestimated, and low turbidity levels of 3–5 FTU were overestimated in the prediction. Conversely, during flood tides, the correlation was approximately 0.98 between the predictions and the actual observations, with only slight underestimation of high turbidity levels, ranging from 100 to 150 FTU, in the observation. Based on these results, it is expected that the poor prediction performance during ebb tide may not be due to the model's failure to replicate predictions. Rather, it seems more likely that the underestimated prediction results are attributed to external factors such as dredging, rather than the effects of tidal variations or stratification and mixing. From this aspect, it appears that during ebb tide, the characteristics of sediment being vertically transported or settling due to the influence of baroclinic currents resulting from strong stratification are relatively well reflected in the training model. During the flood tide, the predicted results showed a turbidity range approximately 10-times higher than those during the ebb tide. This suggests that the resuspension of settled sediments due to strong barotropic currents during flood tide, along with the mixing of water column, was effectively detected by the training model.

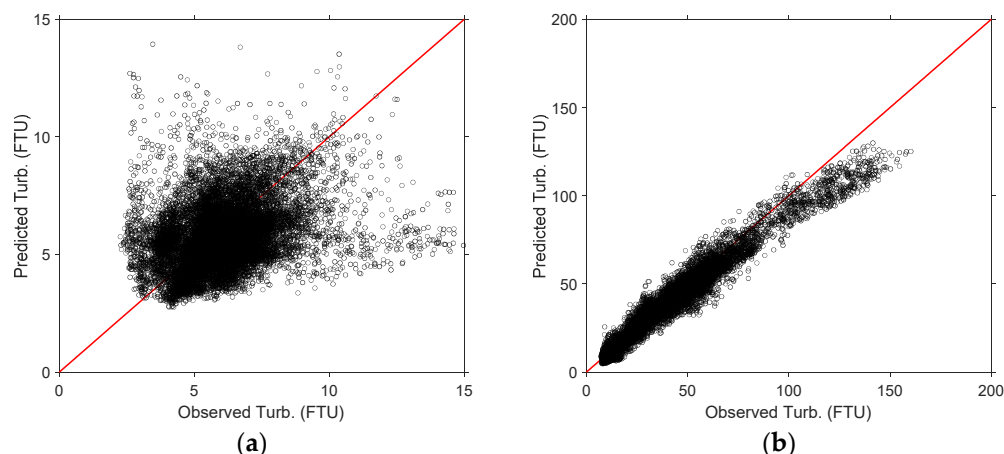


Figure 14. Scatter plot between observed and predicted turbidity during (a) ebb and (b) flood tide.

4. Discussion

The GRE is a semi-enclosed estuary that features transitional zones with freshwater from rivers and saltwater from the ocean. Moreover, the GRE is subjected to tidal influences, but the extent of the tidal impact may be less pronounced than in fully open estuaries due to their partial enclosure. The partial enclosure refers to the intermittent artificial discharge of freshwater, which induces significant changes in the physical and environmental characteristics of the estuary. The combination of restricted water flow and tidal action can lead to unique patterns of sediment deposition (settling) and erosion (resuspension). This can affect the estuary's depth, shape, and the types of habitats available.

To comprehensively understand the characteristics of the GRE, intermittent transect observations were conducted over approximately two years using ADCP and YODA profiler, with 11 sets during ebb tides and 9 during flood tides. The collected data greatly assisted in understanding the vertical distribution characteristics of hydrodynamics and water properties in response to artificial freshwater discharge and the tidal patterns of the estuary. Shortly after the discharge of freshwater, strong stratification occurs, regardless of tidal variations (Figures 5 and 8). This is due to the inertial advection caused by sudden artificial freshwater discharge being stronger than the straining, leading to strong stratification as the freshwater floats along the surface of the navigation channel. Over time, the momentum of the released freshwater weakens, and the tidal modulation begins to dominate, significantly disturbing the water column. Overall, stratification was observed during ebb tides (Figure 6), while mixing characteristics were more prominent during flood tides (Figures 7 and 9). In the GRE, the propagation of the water mass momentum due to tides is blocked by the sea-dike. In particular, during flood tides, the momentum block in front of the sea-dike leads to vertical advection, enhancing the breaking of the stratification, possibly with a periodic process driven by tidal modulation [3,4]. Therefore, irrespective of tidal variations, a general tendency towards mixing was observed in the area in front of the sea-dike.

Notably, during the ebb tide, stratification was intensified, inducing baroclinic currents and, thereby, prompting sediment settling. Conversely, during the flood tide, the observations indicated that barotropic currents, along with mixing, led to the resuspension of sediments. These facts are clearly evident in transect observations conducted in this study, and based on these hydrodynamic characteristics, the machine learning technique was applied to predict the sediment distribution. Out of the 11 ebb tide and 9 flood tide observation profile sets, 10 sets from the ebb tide and 8 sets from the flood tide were used for training, and the last observations from each tidal state were predicted. The machine learning prediction results showed higher accuracy for the condition during flood tides compared to those during ebb tides (Figures 12 and 13). However, this does not imply that the results for ebb tide were incorrect, as the settling characteristics during ebb tides were well simulated. The errors are hypothesized to arise from the model's inability to

accurately simulate the resuspension characteristics of sediments due to dredging or other external factors. In contrast, during flood tides, the resuspension of sediments, enhanced by the turbulent energy of barotropic currents, was very accurately predicted by the machine learning model throughout the observation period. The alignment of the sediment behavior prediction results with theoretical principles in the machine learning model is likely due to the characteristics of the data used as inputs being well reflected in the learning process. In particular, it can be inferred that the currents and density information used as inputs significantly influenced the prediction of sediment deposition (settling) and erosion (resuspension). This inference is based on the fact that estuaries have theoretically defined sediment behavior characteristics, which are affected by hydrodynamics (especially tidal modulation), mixing, and stratification. The data obtained from MVP surveys represent these principles very well. Therefore, it is speculated that this information provided a clear background for sediment behavior in the MLP-NN training process, leading to the theoretically coherent prediction results obtained.

Such kinds of sediment behavior characteristics have been addressed in several previous studies and are an obvious fact that has been theoretically proven [8–10]. Especially, due to the GRE is under the SIPS condition [7], the SIPS mechanism results in maximum buoyancy frequency (N^2) during ebb and minimum N^2 during flood [5]. From the perspective of the Richardson number (Ri_g), it is possible to infer several characteristics of sediment behavior in relation to vertical shear and buoyancy frequency. When Ri_g is less than 0.25, it indicates an actively mixed condition, which means vertical shear (S) dominates over buoyancy (N), suggesting a high likelihood of turbulent mixing. If Ri_g is between 0.25 and 1, it suggests a possibly mixed condition. This range indicates a balance between mixing and stratification, where turbulence is less likely but still possible. The vertical shear-induced turbulent mixing ultimately leads to an enhancement in bottom shear stress, promoting sediments' resuspension [7,19]. When Ri_g is greater than 1, it indicates a stably stratified condition. In this state, buoyancy is stronger than shear forces, suppressing turbulent mixing and maintaining a stable stratified structure in the water column. Therefore, suppressing turbulent mixing ultimately leads to weakening vertical shear, which favors sediment settling over suspension. Reference [7] arrived at conclusions similar to those of this study in the GRE, demonstrating that sediment characteristics during ebb tide are influenced by enhanced stratification and reduced turbulent energy, leading to floc growth and subsequent sediment settling. Conversely, increased turbulent energy and strengthened bottom shear induce sediment resuspension and reduce floc size during the flood tide. This, in turn, leads to the enhancement of the mixing layer and results in sediments remaining suspended for extended periods and undergoing horizontal transport.

Due to the construction of the sea-dike, the sediments in the GRE have transitioned from sandy to muddy, potentially creating an environment more conducive to resuspension during flood tides. Moreover, the intermittent freshwater discharge leads to a substantial sediment influx from the river. The flow velocity decreases in front of the sea-dike, resulting in sediment deposition. The muddy conditions then facilitate the resuspension of these sediments during flood tides, which are subsequently carried out at the sea during ebb tide. This process is likely to cause continuous deposition in the channel of Gunsan Outer Port (Channel 3), which is surrounded by the north breakwater and jetties, thereby necessitating frequent dredging to ensure adequate depth for vessel navigation [20]. During the transect observation, it was readily observed that a dredging vessel, operating continuously, was moored at Channel 1.

The direction of the machine learning model's prediction performance is significantly influenced by the size (duration) and number of input variables. Firstly, the temporal and spatial extent of the input variables, referred to as observations, is a crucial factor in determining how well the model can consider spatiotemporal characteristics. However, unfortunately, studies applying machine learning models solely to observational data from estuaries are scarce, with most utilizing reanalysis, hindcast numerical model data [21], or satellite data [22]. Although there are some studies, even these only deal with training

point-based time-series models [23–25]. The next one is the selection of the number of input variables. In this study, several variables obtainable from the YODA profiler were not included as input data. Notably, water temperature exhibits significant seasonal variations and can detract from prediction performance when used as input data. Therefore, sigma-t, which includes both temperature and salinity information, was predominantly utilized. Additionally, including distance information from the sea-dike as an input value also incorporated locality information into the training process. Since salinity and dissolved oxygen share almost identical structural characteristics with sigma-t, excluding some or including all of these variables does not significantly impact the results. For chlorophyll-a, the relationship between turbidity and chlorophyll-a in estuaries can vary seasonally due to changes in river flows, temperature, and light availability. Spatially, different areas of an estuary (e.g., near the river mouth and closer to the sea) can exhibit different patterns due to variations in salinity, sediment loads, and depth. Tidal modulations can resuspend and settle sediments, affecting turbidity levels. During periods of low turbidity, light penetration improves, potentially enhancing phytoplankton growth. In contrast, high turbidity can limit penetration, which is essential for photosynthesis by phytoplankton, including algae that contain chlorophyll-a. Each estuary is unique, and the specific relationship between turbidity and chlorophyll-a can vary widely based on local conditions and factors. However, based on transect observation results, Chl-a cannot be ignored in the training process due to its non-negligible relationship with turbidity [26], and, thus, it must be considered as an input variable. In addition to those variables, we attempted simulations including the time after freshwater discharge, water level, and upward velocity (VelU) as input variables. However, these variables negatively impacted the predictive results. Consequently, the selection and exclusion of input variables ensured that the machine learning model was robust and capable of accurately predicting turbidity in the GRE by focusing on the most relevant hydrodynamic and environmental factors. The variables, such as time after freshwater discharge, water temperature, and salinity, can be adequately represented by the range of values and vertical structure of sigma-t. Similarly, the velocity structure obtained from ADCP sufficiently reflects the tidal information. Consequently, these variables were subsequently omitted from the simulation process.

Unlike process-based models, which are grounded in theoretical principles and physically and mathematically simulated, data-driven models, especially neural network models such as those used in machine learning, are often perceived as ‘black boxes’ due to their lack of transparency in how decisions or predictions are made. This can be a drawback in settings where understanding the underlying process is as important as the prediction itself. However, data-driven modelling can offer insights into the fundamental processes of phenomena by analyzing the characteristics of input data, thus serving as a valuable tool for hypothesis testing and verification. Furthermore, since process-based models also rely on actual observational data for validation, machine learning models, when trained on empirical data, have the potential to yield results that more closely align with real-world phenomena.

Overall, the transect observations based on the MVP captured instantaneous information on hydrodynamics and water properties and were successful in obtaining observational results that could theoretically validate these aspects. Furthermore, by efficiently organizing this information and applying it to a machine learning model, it was possible to simulate sediment behavior characteristics that can be theoretically derived based on tidal modulations. The construction of the sea-dike caused significant alterations to the circulation and sedimentation in the GRE [27]. These alterations can have profound ecological impacts, affect water quality, and change the morphology of the estuary, which includes the shape and distribution of habitats. Changes in sedimentation and water flow can affect the availability and quality of habitats for estuarine species, including fish, birds, and benthic organisms. This might lead to shifts in species composition and abundance. The changes in circulation can affect the distribution and concentration of nutrients, contaminants, and oxygen levels in the water. This could lead to variations in water quality,

potentially impacting the health of the estuarine ecosystem. Altered sedimentation patterns can impact the quality of sediments, which are crucial for various ecological processes and species. Changes in sediment characteristics can influence the benthic environment and the organisms that rely on it. Therefore, sea-dike and gate operation requires careful consideration and management to balance flood protection with preserving the natural estuarine environment. The insights gained from the MVP surveys and machine learning analysis are instrumental in achieving this balance. The combined use of MVP surveys and machine learning models offers a more sophisticated approach to understanding and managing the GRE. This approach allows for the integration of detailed sediment behavior characteristics into management strategies, ensuring that ecological and environmental impacts are considered alongside flood protection goals.

5. Conclusions

From 2015 to 2017, over a period of two years, transect observations based on the MVP were conducted in the GRE, utilizing both ADCP and YODA profilers mounted simultaneously on a vessel. Based on the acquired observational profile data, a machine learning model was used to predict the structural characteristics of turbidity. The results of this study can be summarized as follows.

- (1) MVP allows for detailed mapping of spatial variations within the estuary and can adapt to changing conditions in real time, which is crucial in dynamic estuarine environments. The MVP in estuaries is a powerful tool for conducting comprehensive and efficient environmental surveys. It provides valuable data for understanding estuarine dynamics, managing resources, and addressing environmental challenges in these complex and critical ecosystems.
- (2) Although the profiles obtained through transect observations represent instantaneous data and are not continuous like time-series observations from fixed stations, there is no alternative method to acquire such high-resolution real measurements of vertical distributions. Therefore, even though the data are captured instantaneously, they can sufficiently interpret the physical and environmental characteristics of the estuary from a theoretical perspective.
- (3) During the ebb tides, sedimentation occurs due to the strengthening of stratification by baroclinic currents, while during flood tides, barotropic currents enhance turbulent shear forces, resulting in the resuspension and suspension of sediments. The theoretical background of these sediment behavior characteristics is well reflected in the profile data, and the results predicted by the machine learning model based on these data were also found to be quite accurate.

It is evident that a simple MLP-NN model can produce sufficiently accurate results with just information on tidal current variations and the stratification and mixing characteristics of the water column. However, additional study is needed to address tendencies of over- or under-estimation in the model. Securing longer-term observation data or input data for training based on the hindcast numerical modeling could enable the interpretation of problems from a longer time-scale perspective, not just limited to ebb and flood but also including neap and spring tides. Furthermore, as more data accumulate, efforts should be made to reduce simulation time for the model and to construct deeper and more profound neural networks, such as those based on CNN (Convolutional Neural Network) or LSTM (Long Short-Term Memory). Particularly, the MLP-NN model's flexibility is needed through the optimization of hyperparameters and setups like transfer functions or minibatch training.

Author Contributions: Conceptualization, N.-H.K.; methodology, N.-H.K. and S.-H.P.; data acquisition, N.-H.K. and D.H.K.; data curation, N.-H.K.; writing—original draft preparation, N.-H.K.; writing—review and editing, N.-H.K., D.H.K. and S.-H.P. All authors have read and agreed to the published version of the manuscript.

Funding: This research was supported by an in-house grant from KIOST (PEA0142, Research of prediction techniques to reduce damage from marine disasters).

Data Availability Statement: The data used in this study are available on request from the corresponding author.

Conflicts of Interest: The authors declare no conflicts of interest.

Appendix A

Table A1. Detailed information of the freshwater discharge (W.L.: Water Level).

Date	Start Time	End Time	Start W.L. (m)	End W.L. (m)	Amount of Discharge (ton)
2015.03.13.	09:23	14:05	1.67	0.12	45,885
2015.04.10.	08:44	10:50	1.70	0.70	30,510
2015.08.21.	05:51	10:19	1.68	1.23	14,059
2016.01.08.	16:46	18:55	1.60	0.55	31,655
2016.08.29.	13:48	15:45	1.97	1.61	11,579
2016.09.01.	17:36	20:01	1.91	1.28	19,926
2016.11.07.	09:03	11:26	1.81	1.07	23,085
2016.11.10.	12:13	15:26	1.55	0.82	22,245
2017.01.06.	09:43	12:55	1.87	0.98	27,724
2017.01.10.	15:45	17:57	1.62	0.93	21,204

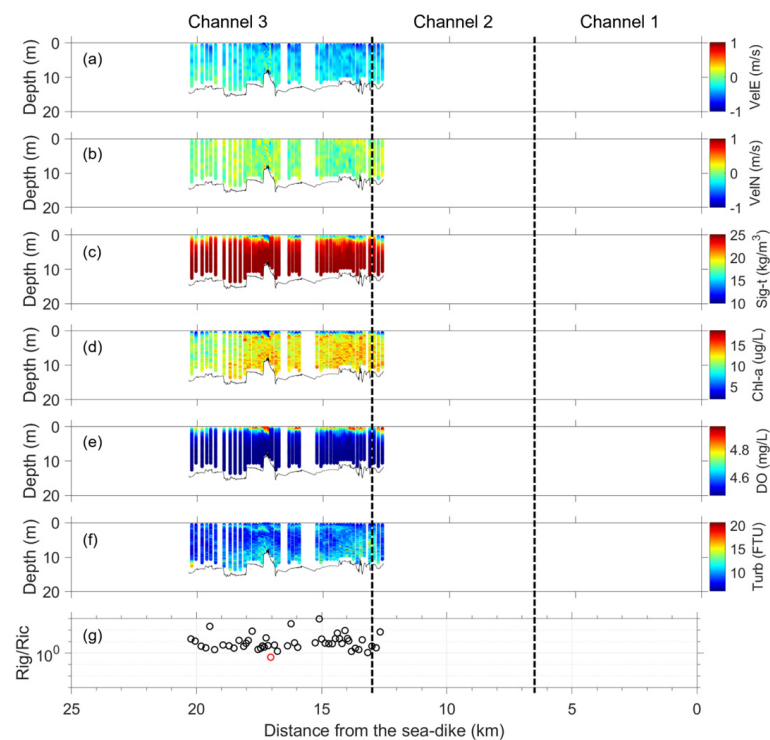


Figure A1. (a–f) Vertical profiles acquired 26 h after freshwater discharge through the transect observation based on MVP method during the ebb tide (14 March 2015). (g) The gradient Richardson number (Ri_g/Ric), where red dots represent possibly mixed conditions, and black dots denote stably stratified conditions.

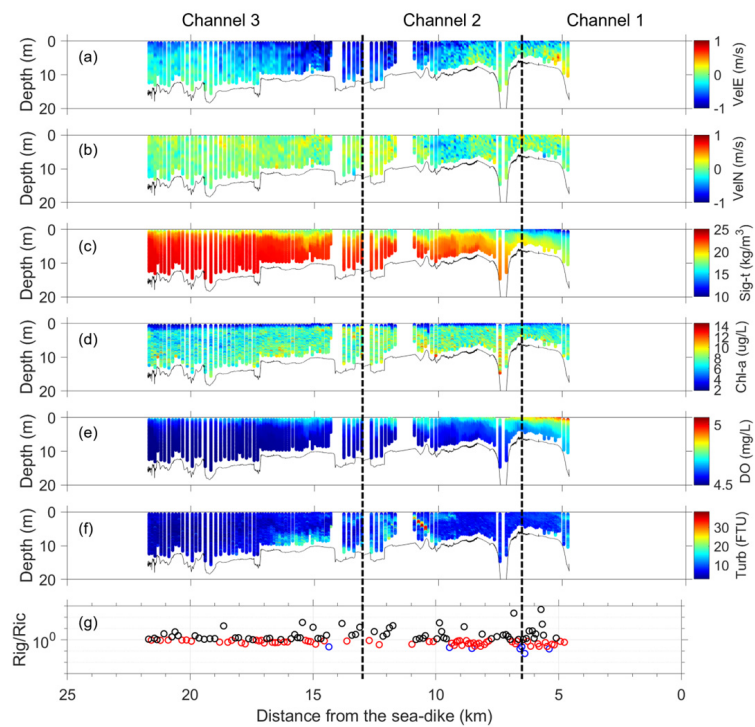


Figure A2. (a–f) Vertical profiles acquired 24 h after freshwater discharge through the transect observation based on MVP method during the ebb tide (11 April 2015). (g) The gradient Richardson number (Ri_g), where blue dots indicate actively mixed conditions, red dots represent possibly mixed conditions, and black dots denote stably stratified conditions.

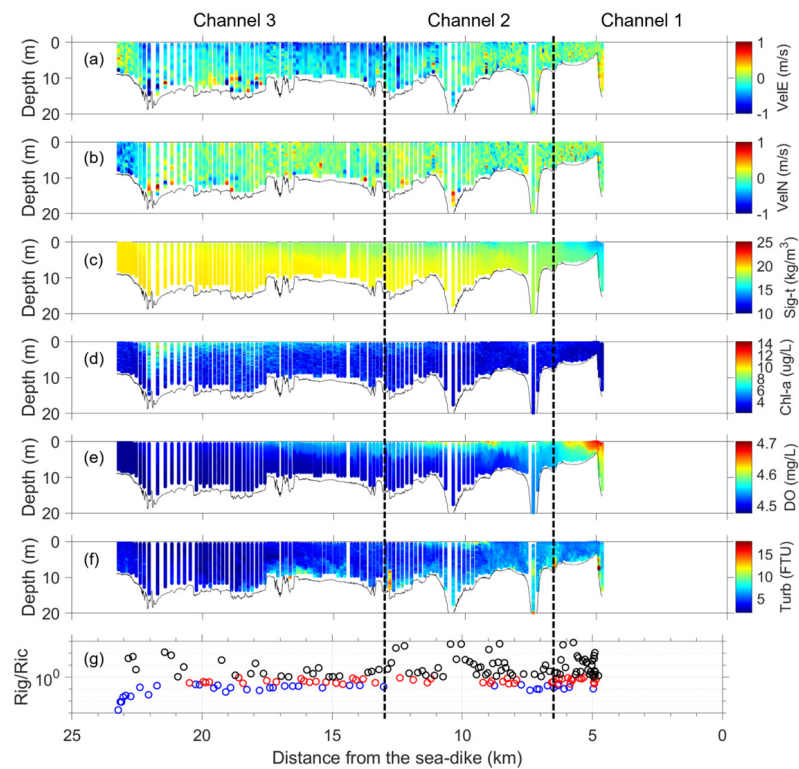


Figure A3. (a–f) Vertical profiles acquired 72 h after freshwater discharge through the transect observation based on MVP method during the ebb tide (24 August 2015). (g) The gradient Richardson number (Ri_g), where blue dots indicate actively mixed conditions, red dots represent possibly mixed conditions, and black dots denote stably stratified conditions.

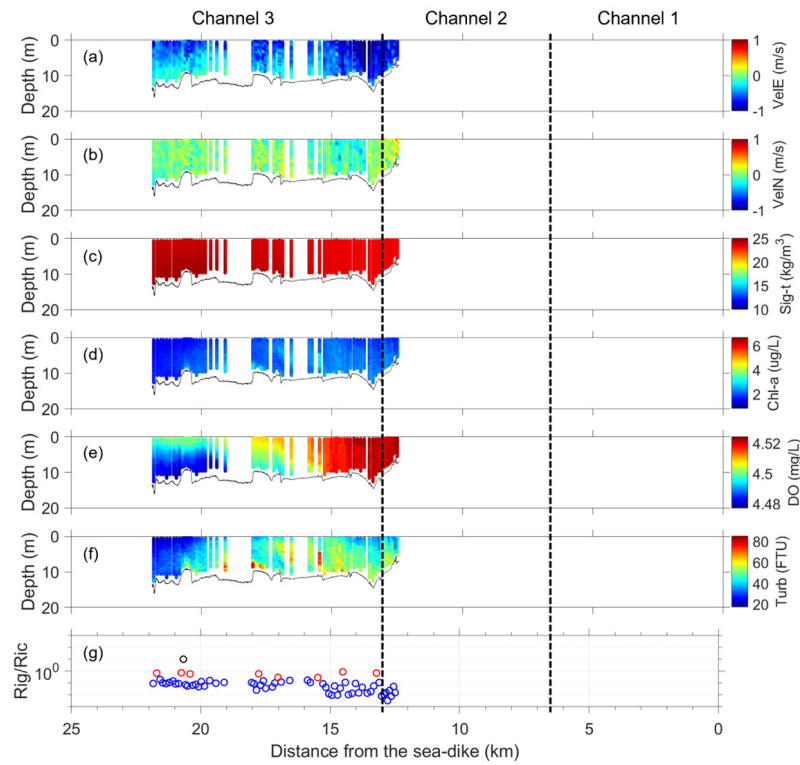


Figure A4. (a–f) Vertical profiles acquired 129 h after freshwater discharge through the transect observation based on MVP method during the ebb tide (14 January 2016). (g) The gradient Richardson number (Ri_g), where blue dots indicate actively mixed conditions, red dots represent possibly mixed conditions, and black dots denote stably stratified conditions.

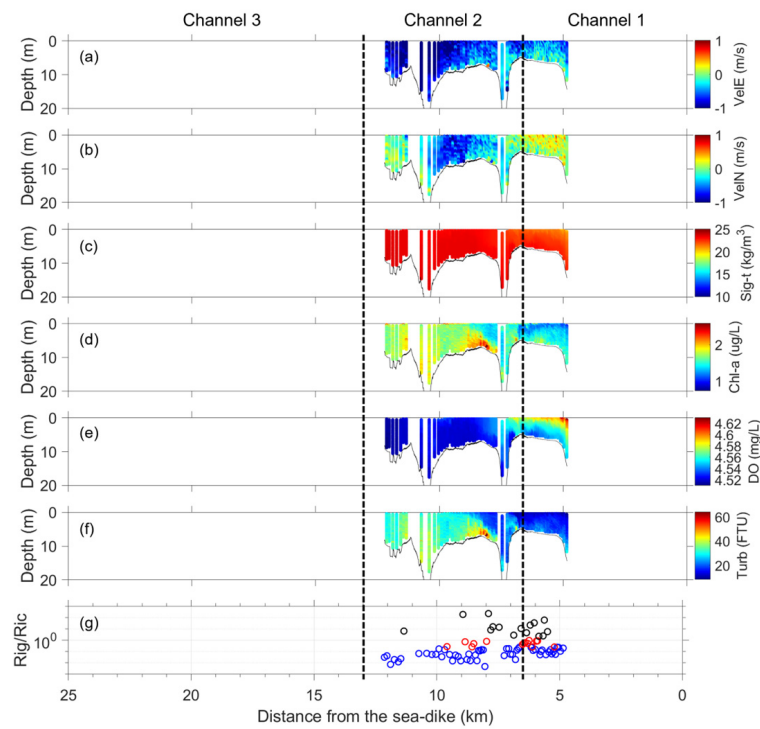


Figure A5. (a–f) Vertical profiles acquired 153 h after freshwater discharge through the transect observation based on MVP method during the ebb tide (15 January 2016). (g) The gradient Richardson number (Ri_g), where blue dots indicate actively mixed conditions, red dots represent possibly mixed conditions, and black dots denote stably stratified conditions.

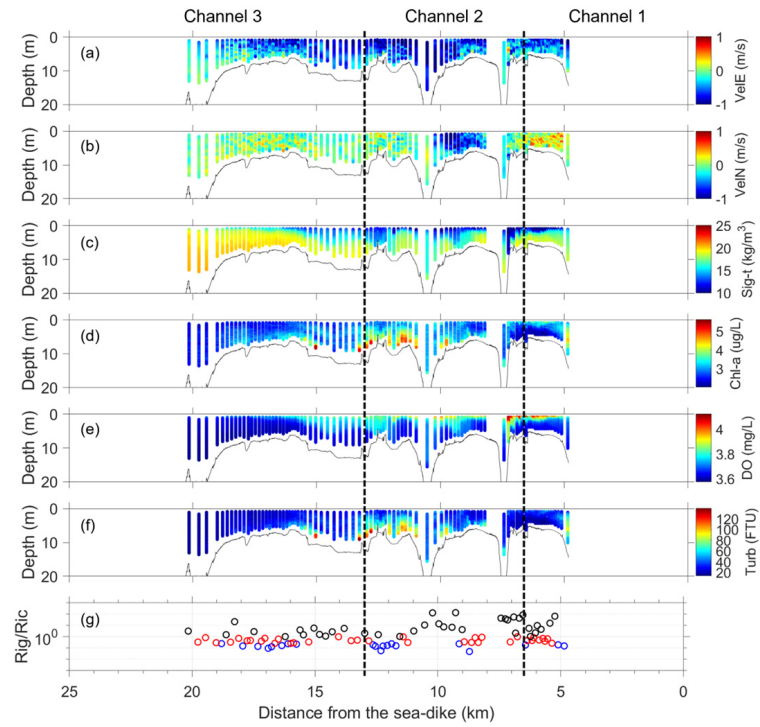


Figure A6. (a–f) Vertical profiles acquired 11 h after freshwater discharge through the transect observation based on MVP method during the ebb tide (2 September 2016). (g) The gradient Richardson number (Ri_g), where blue dots indicate actively mixed conditions, red dots represent possibly mixed conditions, and black dots denote stably stratified conditions.

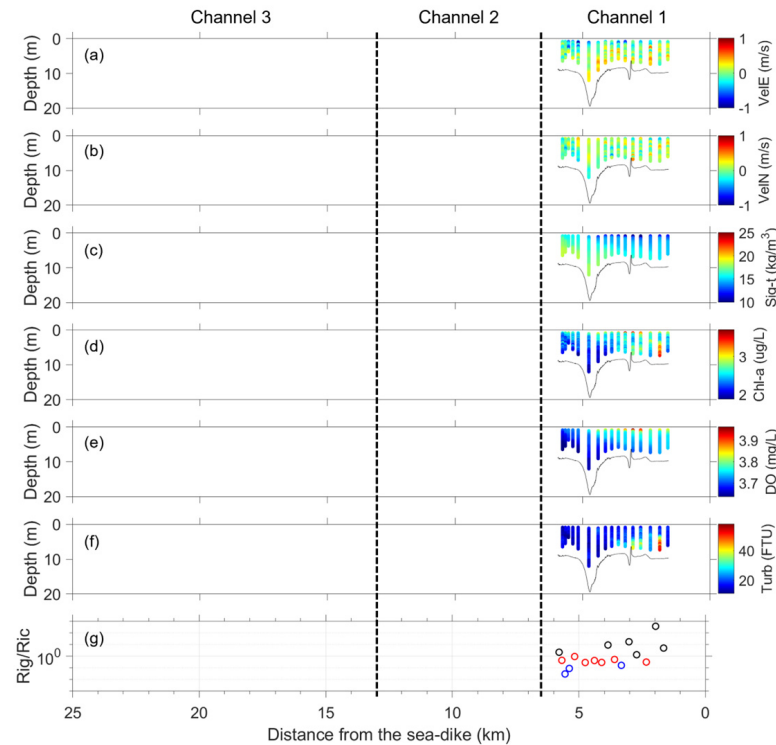


Figure A7. (a–f) Vertical profiles acquired 19 h after freshwater discharge through the transect observation based on MVP method during the ebb tide (2 September 2016). (g) The gradient Richardson number (Ri_g), where blue dots indicate actively mixed conditions, red dots represent possibly mixed conditions, and black dots denote stably stratified conditions.

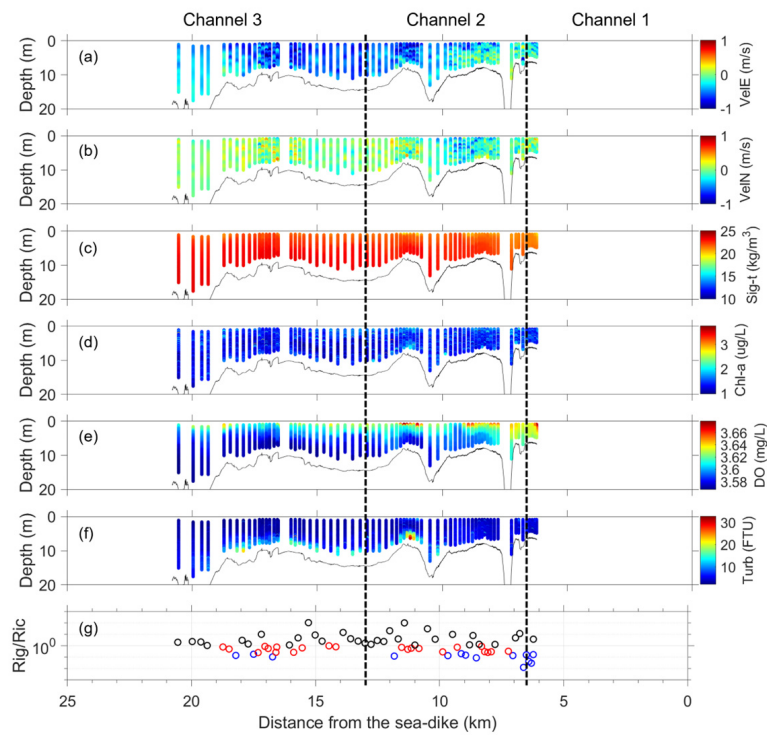


Figure A8. (a–f) Vertical profiles acquired 75 h after freshwater discharge through the transect observation based on MVP method during the ebb tide (10 November 2016). (g) The gradient Richardson number (Ri_g), where blue dots indicate actively mixed conditions, red dots represent possibly mixed conditions, and black dots denote stably stratified conditions.

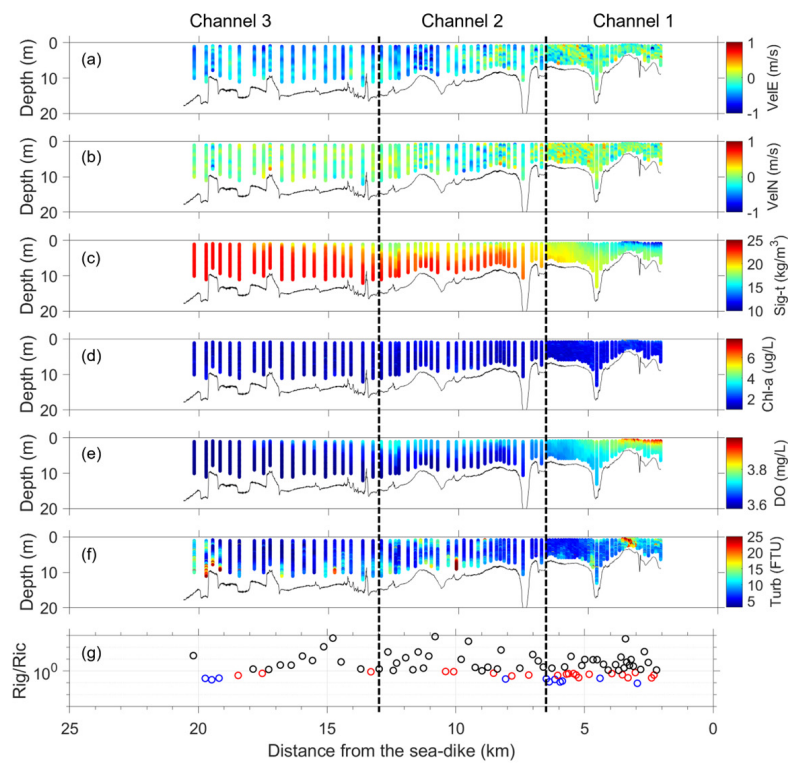


Figure A9. (a–f) Vertical profiles acquired 24 h after freshwater discharge through the transect observation based on MVP method during the ebb tide (11 November 2016). (g) The gradient Richardson number (Ri_g), where blue dots indicate actively mixed conditions, red dots represent possibly mixed conditions, and black dots denote stably stratified conditions.

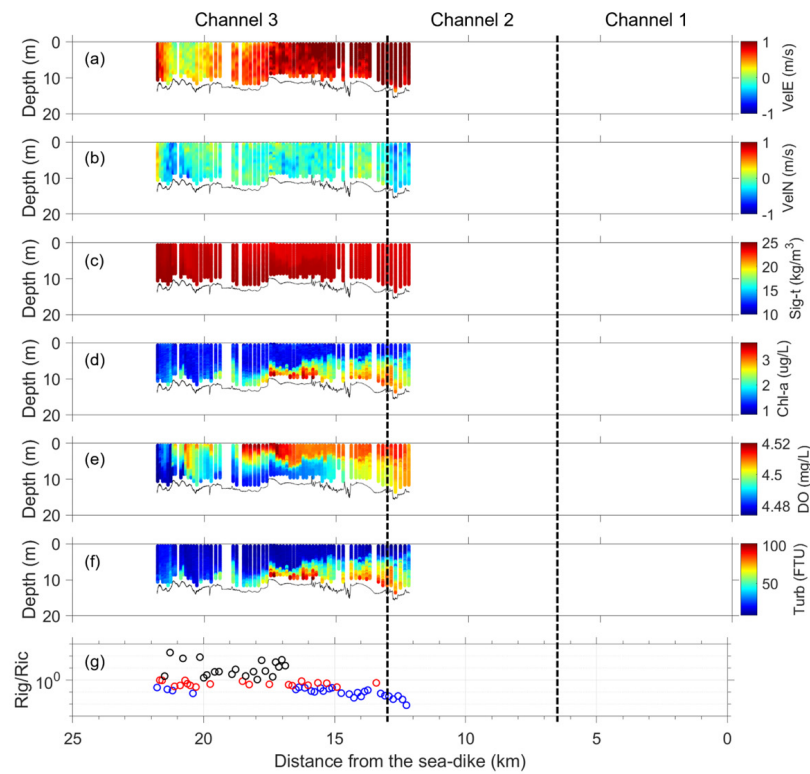


Figure A10. (a–f) Vertical profiles acquired 133 h after freshwater discharge through the transect observation based on MVP method during the flood tide (14 January 2016). (g) The gradient Richardson number (Ri_g), where blue dots indicate actively mixed conditions, red dots represent possibly mixed conditions, and black dots denote stably stratified conditions.

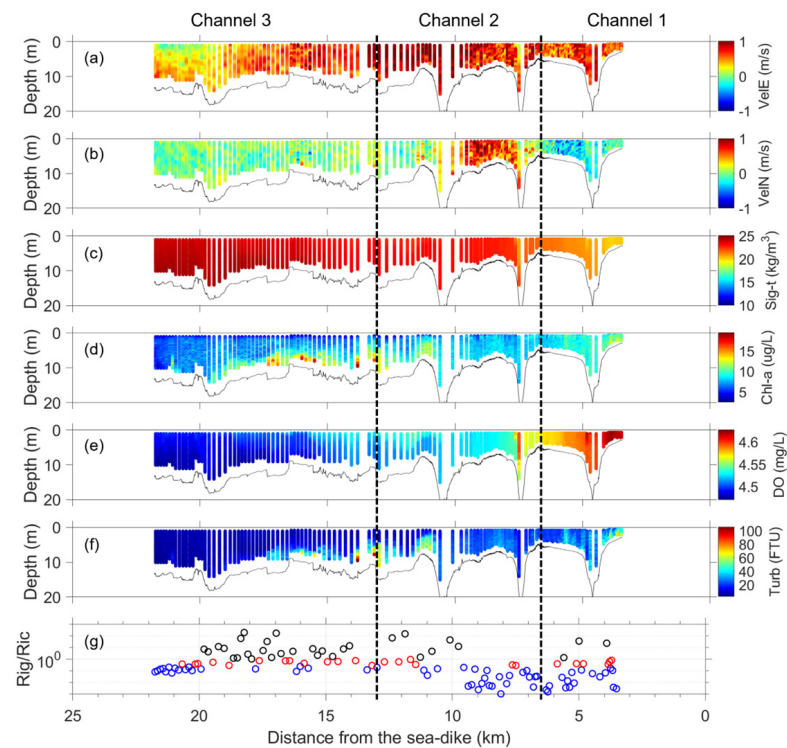


Figure A11. (a–f) Vertical profiles acquired 133 h after freshwater discharge through the transect observation based on MVP method during the flood tide (22 March 2016). (g) The gradient Richardson number (Ri_g), where blue dots indicate actively mixed conditions, red dots represent possibly mixed conditions, and black dots denote stably stratified conditions.

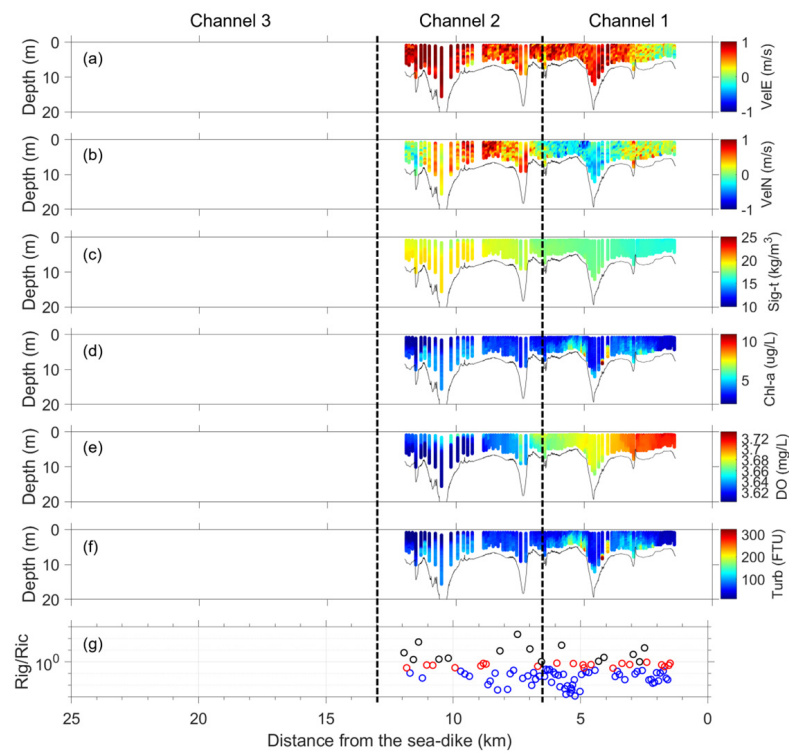


Figure A12. (a–f) Vertical profiles acquired 70 h after freshwater discharge through the transect observation based on MVP method during the flood tide (1 September 2016). (g) The gradient Richardson number (Ri_g), where blue dots indicate actively mixed conditions, red dots represent possibly mixed conditions, and black dots denote stably stratified conditions.

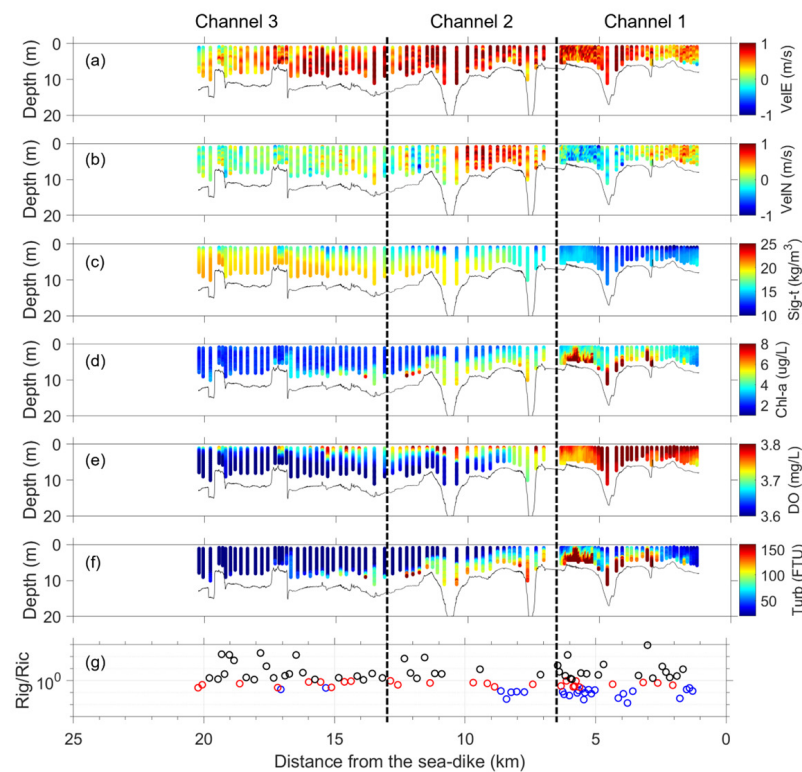


Figure A13. (a–f) Vertical profiles acquired 15 h after freshwater discharge through the transect observation based on MVP method during the flood tide (2 September 2016). (g) The gradient Richardson number (Ri_g), where blue dots indicate actively mixed conditions, red dots represent possibly mixed conditions, and black dots denote stably stratified conditions.

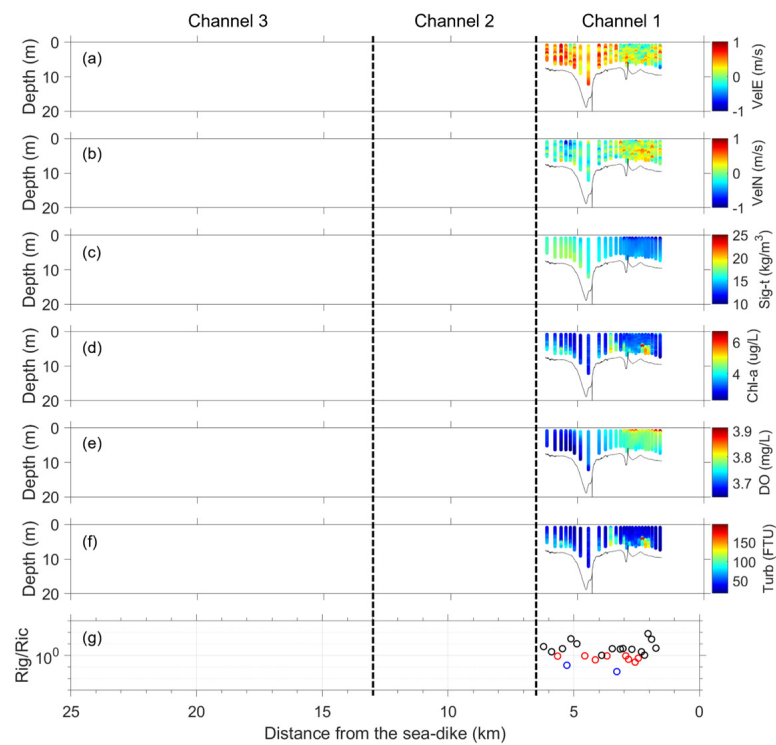


Figure A14. (a–f) Vertical profiles acquired 18 h after freshwater discharge through the transect observation based on MVP method during the flood tide (2 September 2016). (g) The gradient Richardson number (Ri_g), where blue dots indicate actively mixed conditions, red dots represent possibly mixed conditions, and black dots denote stably stratified conditions.

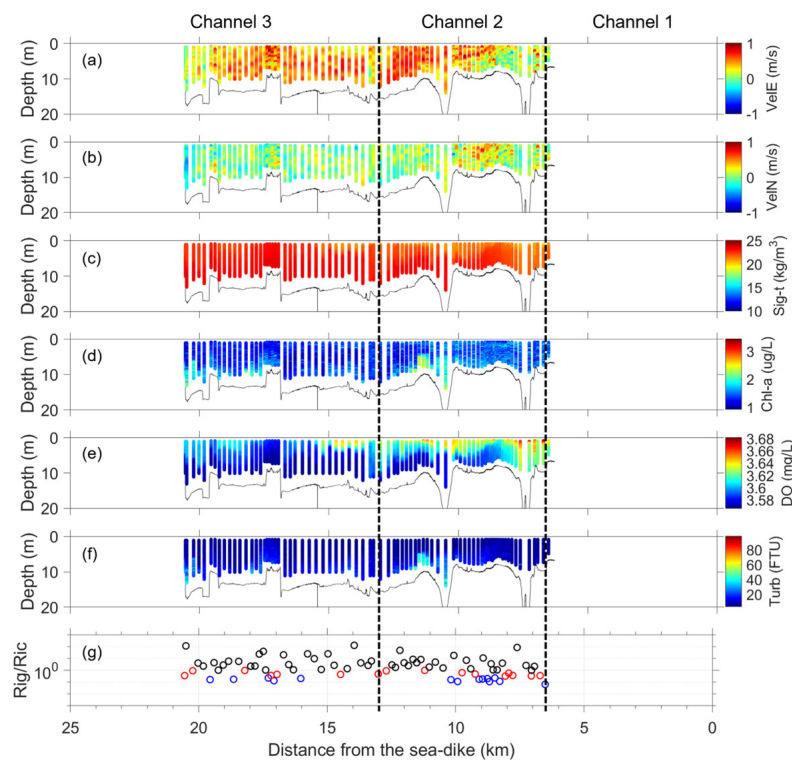


Figure A15. (a–f) Vertical profiles acquired 71 h after freshwater discharge through the transect observation based on MVP method during the flood tide (10 November 2016). (g) The gradient Richardson number (Ri_g), where blue dots indicate actively mixed conditions, red dots represent possibly mixed conditions, and black dots denote stably stratified conditions.

References

1. Kim, N.H.; Hwang, J.H. Optimal Design of Water Quality Monitoring Networks in Semi-Enclosed Estuaries. *Sensors* **2020**, *20*, 1498. [[CrossRef](#)] [[PubMed](#)]
2. Simpson, J.H. Physical Processes in the ROFI Regime. *J. Mar. Syst.* **1997**, *12*, 3–15. [[CrossRef](#)]
3. Kim, N.H.; Hwang, J.H.; Dong Hyeon, K. Evaluation of Mixing and Stratification in an Estuary of Korea. *J. Coast. Res.* **2018**, *SI85*, 96–100. [[CrossRef](#)]
4. Kim, N.H.; Hwang, J.H.; Ku, H. Stratification of Tidal Influenced Navigation Channel. *J. Coast. Res.* **2016**, *SI75*, 63–67. [[CrossRef](#)]
5. Simpson, J.H.; Brown, J.; Matthews, J.; Allen, G. Tidal Straining, Density Currents, and Stirring in the Control of Estuarine Stratification. *Estuaries* **1990**, *13*, 125–132. [[CrossRef](#)]
6. Figueroa, S.M.; Lee, G.; Shin, H.J. Effects of an Estuarine Dam on Sediment Flux Mechanisms in a Shallow, Macrotidal Estuary. *Estuar. Coast. Shelf. Sci.* **2020**, *238*, 106718. [[CrossRef](#)]
7. Figueroa, S.M.; Lee, G.; Shin, H.J. The Effect of Periodic Stratification on Floc Size Distribution and Its Tidal and Vertical Variability: Geum Estuary, South Korea. *Mar. Geol.* **2019**, *412*, 187–198. [[CrossRef](#)]
8. Scully, M.E.; Friedrichs, C.T. The Importance of Tidal and Lateral Asymmetries in Stratification to Residual Circulation in Partially Mixed Estuaries. *J. Phys. Oceanogr.* **2007**, *37*, 1496–1511. [[CrossRef](#)]
9. Burchard, H.; Schuttelaars, H.M.; Ralston, D.K. Sediment Trapping in Estuaries. *Annu. Rev. Mar. Sci.* **2018**, *10*, 371–395. [[CrossRef](#)]
10. Lee, B.J.; Fettweis, M.; Toorman, E.; Molz, F.J. Multimodality of a Particle Size Distribution of Cohesive Suspended Particulate Matters in a Coastal Zone. *J. Geophys. Res. Oceans* **2012**, *117*, C03014. [[CrossRef](#)]
11. Kim, T.I.; Choi, B.H.; Lee, S.W. Hydrodynamics and Sedimentation Induced by Large-Scale Coastal Developments in the Keum River Estuary, Korea. *Estuar. Coast. Shelf. Sci.* **2006**, *68*, 515–528. [[CrossRef](#)]
12. Kim, N.H.; Hwang, J.H.; Cho, J.; Kim, J.S. A Framework to Determine the Locations of the Environmental Monitoring in an Estuary of the Yellow Sea. *Environ. Pollut.* **2018**, *241*, 576–585. [[CrossRef](#)] [[PubMed](#)]
13. Lee, J.; Lee, J. An Analytical Study on Heavy Siltation in the Keum River Estuary after the Construction of a Dyke. *J. Coast. Res.* **2007**, *SI50*, 1147–1151.
14. Kim, D.H.; Hwang, J.H. Estimating Bed Shear Stress Distribution over Bottom of a Channel on the Moving Vessel. *Ocean Sci. J.* **2023**, *58*, 3. [[CrossRef](#)]
15. Kim, D.H.; Hwang, J.H.; Jeong, J.; Hong, Y.; Lee, M. Comprehensive Modeling from Watersheds to a Bay and Its Validation with Radar, Drifters, and MVP Methods. *Reg. Stud. Mar. Sci.* **2023**, *68*, 103262. [[CrossRef](#)]
16. Masunaga, E.; Yamazaki, H. A New Tow-Yo Instrument to Observe High-Resolution Coastal Phenomena. *J. Mar. Syst.* **2014**, *129*, 425–436. [[CrossRef](#)]
17. Miles, J.W. On the Stability of Heterogeneous Shear Flows. *J. Fluid. Mech.* **1961**, *10*, 496–508. [[CrossRef](#)]
18. Giddings, S.N.; Fong, D.A.; Monismith, S.G. Role of Straining and Advection in the Intratidal Evolution of Stratification, Vertical Mixing, and Longitudinal Dispersion of a Shallow, Macrotidal, Salt Wedge Estuary. *J. Geophys. Res. Oceans* **2011**, *116*, C03003. [[CrossRef](#)]
19. Jay, D.A.; Musiak, J.D. Internal Tidal Asymmetry in Channel Flows: Origins and Consequences. *Mix. Estuaries Coast. Seas* **1996**, *50*, 211–249. [[CrossRef](#)]
20. Shin, M.-S.; Bae, K.S.; Kang, S.J.; Kim, J.H. A Study on the Topography and Current Characteristic of the before and after Construction at Geum River Estuary Dike. *J. Ocean. Eng. Technol.* **2006**, *20*, 61–66. (In Korean, with English Abstract)
21. Luo, Y.; Shi, H.; Zhang, Z.; Zhang, C.; Zhou, W.; Pan, G.; Wang, W. Wave Field Predictions Using a Multi-Layer Perceptron and Decision Tree Model Based on Physical Principles: A Case Study at the Pearl River Estuary. *Ocean Eng.* **2023**, *277*, 114246. [[CrossRef](#)]
22. Huang, Y.; Pan, J.; Devlin, A.T. Enhanced Estimate of Chromophoric Dissolved Organic Matter Using Machine Learning Algorithms from Landsat-8 OLI Data in the Pearl River Estuary. *Remote Sens.* **2023**, *15*, 1963. [[CrossRef](#)]
23. Guillou, N.; Chapalain, G. Machine Learning Methods Applied to Sea Level Predictions in the Upper Part of a Tidal Estuary. *Oceanologia* **2021**, *63*, 531–544. [[CrossRef](#)]
24. Cigizoglu, H.K. Estimation and Forecasting of Daily Suspended Sediment Data by Multi-Layer Perceptrons. *Adv. Water Resour.* **2004**, *27*, 185–195. [[CrossRef](#)]
25. Pektas, A.O.; Cigizoglu, H.K. Long-Range Forecasting of Suspended Sediment. *Hydrol. Sci. J.* **2017**, *62*, 2415–2425. [[CrossRef](#)]
26. McSweeney, J.M.; Chant, R.J.; Wilkin, J.L.; Sommerfield, C.K. Suspended-Sediment Impacts on Light-Limited Productivity in the Delaware Estuary. *Estuaries Coast.* **2017**, *40*, 977–993. [[CrossRef](#)]
27. Figueroa, S.M.; Lee, G.H.; Chang, J.; Jung, N.W. Impact of Estuarine Dams on the Estuarine Parameter Space and Sediment Flux Decomposition: Idealized Numerical Modeling Study. *J. Geophys. Res. Oceans* **2022**, *127*, e2021JC017829. [[CrossRef](#)]

Disclaimer/Publisher’s Note: The statements, opinions and data contained in all publications are solely those of the individual author(s) and contributor(s) and not of MDPI and/or the editor(s). MDPI and/or the editor(s) disclaim responsibility for any injury to people or property resulting from any ideas, methods, instructions or products referred to in the content.